UNIVERSIDAD NACIONAL DE COLOMBIA

Modelo para la atenuación de la velocidad de flujo dentro de pastos marinos

Johann Khamil Delgado Gallego

Universidad Nacional de Colombia, Sede Medellín
Facultad de Minas, Departamento de Geociencias y Medio Ambiente
Medellín, Colombia
2019

In-canopy Velocity Attenuation in a Model of Submerged Vegetation

Johann Khamil Delgado Gallego

Master of Engineering - Hydraulic Resources

Advisor:
Ph.D. Andrés Fernando Osorio

Co-Advisor:
Ph.D. Francisco Mauricio Toro

Research Field:
Coastal Engineering
Research Group OCEANICOS

National University of Colombia at Medellín
Faculty of Mines, Department of Geoscience and Environment
Medellín, Colombia
2019

Content

List of figures

List of tables

1 Resumen - Abstract

Título: Modelo para la atenuación de lavelocidad de flujo dentro de pastosmarinos.

Se desarrolla un modelo para la disipación de la energía del oleaje en presencia de pastos marinos con flexibilidad inetrmedia que presenten movimientos tipo 'viga Cantilever'. Los resultados del modelo muestran mejoras significativas en comparación a los resultados obtenidos considerando la vegetación como rigida. Se calcularon los coeficientes de atenuación de la velocidad del flujo al inerior del pastizal.

Title: In-canopy Velocity Attenuation in a Model of Submerged Vegetation

A model is developed for the dissipation of wave energy in the presence of seagrasses with intermediate flexibility that present Cantilever beam'movements. The model results show significant improvements compared to the results obtained considering the vegetation as rigid. The attenuation coefficients of the flow velocity inside the grassland were calculated.

2 Introduction

Submerged vegetation is extremely relevant for the human development. Several coastal zones worldwide are provided by seagrasses, which protect the coast from the adverse effects of waves during mean and extreme conditions. In addition, this ecosystems provide important ecological services and economic benefits to society (Moberg y Folke, 1999). Seagrasses act on water flow reducing currents close to the seabed and hence, limiting the sediment transport(Luhar et al., 2017).

Previous studies have addressed the interaction seagrass-oscillatory-flow with the aim to understand and estimate the rate of wave energy dissipation that takes place within the ecosystems. They have shown that this process is mainly dependant on the wave incident conditions and the vegetation features such as vegetation density, flexibility, and plant morphology. However, an important number of studies assume that the interaction plant-flow does not generate a transformation in the velocity patterns and in the plant position, that is to say, the structures are rigid and the velocity profile is not attenuated.

These assumptions contradict observations that have been made both in the field and in the laboratory through the use of physical models. These formulations, trying to provide results that fit the experimental data, have used empirical coefficients (e.g. drag coefficient, C_D) as a parameter for refining the results.

As an alternative to estimate energy dissipation in the presence of flexible vegetation, recently Luhar y Nepf (2011) y Luhar y Nepf (2016) introduced the concept of equivalent length (l_e), which can be defined as the length that a rigid element would have so that it generates the same dissipation as the flexible element, which would generally be greater than the rigid one. Additionally, to take into account the presence of the vegetation and its effect on the flow patterns, Lei y Nepf (2019) considered the attenuation of the in-canopy velocity using the attenuation coefficient (α_w) developed by Lowe et al. (2005), which relates the magnitude of the velocity inside and outside the vegetation. However, the calculation of this coefficient is based, *again*, on the hypothesis that the elements are rigid.

On the other hand, some studies have represented the flow-structure interaction through the coupling between the equations that govern the flow and the movement of vegetation. To achieve this, seagrass has been modelled both as a Cantilever beam and as an element with

a whip movement, according to the conditions of flexibility that the seagrass possesses. To establish the movement of the fluid 'CFD' (*Computational Fluid Dynamics*) models have been used, which solve the equations of fluid governance on small spatial scales($\sim 10^{-3}\, m$) (e.g. Maza et al. (2013) y Pujol et al. (2013)). However, they have a significantly greater complexity than the models used by Lei y Nepf (2019), making them technically inconvenient due to the large computational effort that they require.

3 Objectives

3.1. General

To study the effect of flexibility of seagrasses on the wave energy dissipation

3.2. Specifics

- Identify the forces that disturb and restore the movement of the seagrass blades.
- Develop a mathematical model of the wave energy dissipation, which consider the seagrasses as flexible structures.
- Identify the geometrical, physical, and mechanic characteristics of seagrasses that have a key influence on wave energy dissipation.

4 State of the Art

4.1. Wave Energy Attenuation

Aquatic vegetation is often characterised of providing important services to coastal ecosystems and human communities, such as habitat and shelter for many species of fishes and other aquatic life, and reduction of wave-driven flows that impact the sediment transport. Seagrasses attenuate incoming waves and protect shorelines from erosion, reduce resuspension of particulate material and enhance sedimentation (Abdolahpour et al., 2018). Additionally, they stabilise the seabed and improve water clarity, which leads to greater light penetration and increased productivity (Gruber et al., 2011).

A number of studies has examined the attenuation of wave energy by submerged real vegetation (Bradley y Houser, 2009) or parameterizations such as cylinders and plates to mimic the seagrass in the laboratory (Houser et al., 2014; Lei y Nepf, 2019; Luhar et al., 2017). Generally, it is assumed that the linear wave theory is valid and thus, it is possible to use this theory to describe the variation of wave-energy flux, ($E_w c_g$), it is the rate at which the fluid makes work on an arbitrary vertical section (Dean y Dalrymple, 1989). The wave-energy flux can be modified by, for instance, transformation processes due to interactions with seabead, such as shoaling, bottom friction, wave breaking or vegetation-flow interaction. Here, we assume that there is only transformation due to vegetation-flow interaction:

$$\frac{\partial E_w\, c_g}{\partial x} = -\varepsilon_v \tag{4.1}$$

where E_w is the wave energy density, c_g is the group velocity, and ε_v is the rate of wave-energy dissipation per unit plan area of an oscillatory flow propagating over a vegetated rough surface. Considering only drag forces, Dalrymple et al. (1984) presented a formulation to estimate ε_v (Mendez y Losada, 2004):

$$\varepsilon_v = \frac{2}{3\pi}\rho\, C_D b_v N \left(\frac{kg}{2\omega}\right)^3 \frac{\sinh^3 kh_v + 3\sinh kh_v}{3k\cosh^3 kh} H^3 \tag{4.2}$$

where ρ is the water density, C_D is the drag coefficient, b_v is the plant width normal to the flow, N is the density of blades ($blades\, m^{-2}$), $k = 2\pi/\lambda$ is the wave number based on the

wave length λ, g is the acceleration due to gravity, ω is the angular wave frequency, h_v is the vegetation height, h is the still water depth, and H is the wave height. Combining equations (4.1 and 4.2) and solving, a solution of the following form is achieved:

$$\frac{H}{H_0} = \frac{1}{1 + K_D H_0 x} \tag{4.3}$$

Here, H_0 is the wave height at the beginning of the meadow, $x = 0$, and K_D is a wave decay coefficient, defined as:

$$K_D = \frac{2}{9\pi} C_D b_v N k \left[\frac{9\sin(kh_v) + \sinh(3kh_v)}{\sinh(kh)\sinh(2kh) + 2kh_v} \right] \tag{4.4}$$

However, some pivotal assumptions were considered to develop this expression: i) vegetation motion such as vibration due to vortices and swaying was neglected; and ii) fluid velocity over the entire water depth is given by linear wave theory (U_∞) and iii) local flow field inside a canopy is not modified by the presence of the canopy elements (Lowe et al., 2007; Luhar et al., 2017). Conversely, recent studies have shown that the plant movement has a critical participation on wave-energy attenuation mainly by reducing drag coefficients (Abdolahpour et al., 2017a; Houser et al., 2014; Zhu y Chen, 2015). Moreover, experiments employing submerged vegetation show a significant attenuation for the in-canopy wave velocity (Lowe et al., 2005; Abdolahpour et al., 2018). The figure (4.1) shows a theoretical typical velocity profile, characterised by the root-mean-square (rms) velocities above (∞) and within (w) the vegetation. The equation (4.5) defines the incident velocity dictated by linear theory:

$$U_\infty = \frac{H}{2}\omega \frac{\cosh kz}{\sinh kh} \sin \omega t \tag{4.5}$$

Note that z represents the vertical coordinate ($z = 0$ at the bed) and t denotes time. On the vicinity of the vegetation top, the velocity is accelerated as a consequence of the discontinuity in the momentum balance generating the formation of a skimming flow (Maza et al., 2013), which has critical participation in mass exchange and vortex shedding.

As an alternative to estimate wave-energy attenuation with flexible vegetation (e.g., seagrass), via equation (4.2), Luhar et al. (2017) employed an effective blade length l_e, which is defined as the rigid blade length that dissipates the same wave-energy as the moving flexible blade, replacing h_v by the effective length l_e in equation (4.2). Then, the equation (4.6) is rewritten as:

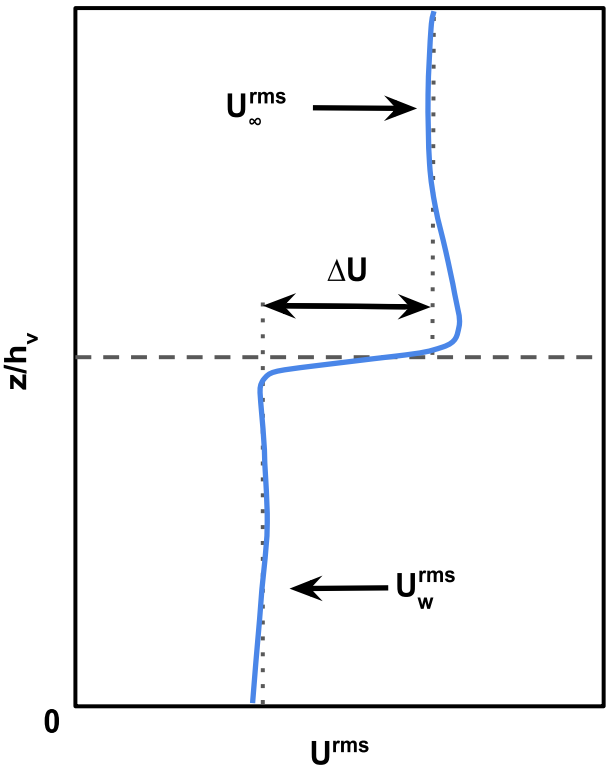

Figure 4.1: Blue solid line represents a typical velocity profile of the experiments considered in this study. Dot lines are overlapping to indicate mean values of the incident (U_{∞}^{rms}) and in-canopy (U_{w}^{rms}) velocities

$$K_D = \frac{2}{9\pi} C_D b_v N k\, \alpha_w^3 \left[\frac{9\sin(kl_e) + \sinh(3kl_e)}{\sinh(kh)\sinh(2kh) + 2kh_v} \right] \tag{4.6}$$

Previously, Luhar y Nepf (2016) showed that l_e depends primarily on two dimensionless parameters: i) the Cauchy number, Ca, which represents the ratio of the hydrodynamic forcing to the restoring force due to blade stiffness and ii) the ratio of blade length to wave excursion, L, which are defined as:

$$Ca = \frac{\rho\, b_v \left(U_\infty^{max}\right)^2 h_v^3}{EI} \tag{4.7}$$

here U_∞^{max} is assumed as the characteristic velocity; E is the elastic modulus of the blade, and $I = b_v t_v^3/12$ is the second moment of area for the blade cross-section, where t_v is blade thickness. The length ratio is defined as:

$$L = \frac{h_v}{A_\infty} \tag{4.8}$$

When the drag force is much smaller than the restoring force due to stiffness $Ca \ll 1$, the plant remains upright in the flow. Whereas $Ca > 1$, vegetation stars to sway and the hydrodynamic forces becomes larger than the restoring forces, e.g. stiffness and buoyancy. For $L \ll 1$ unsteady flow with large excursions are presented, so the wave excursion becomes much greater than the blade length and vegetation trends a posture as figure (4.2a) shows. For $L \gg 1$, the horizontal wave excursion is much smaller than the blade length, so the blade remains nearly vertical as it moves back and forth throughout the wave cycle (4.2b) (Luhar y Nepf, 2016).

Combining the two dimensionless parameters ($Ca\, L$), seagrasses could be differentiated from extremely stiff vegetation when the plant stem barely moves in the water, to extremely flexible vegetation when the stem follows the movement of surrounding water particles, ranging from $Ca\, L \sim 10^{-1} - 10^5$ (Zhu y Chen, 2015; Lei y Nepf, 2019). For $Ca\, L < 10^3$ plant motion can be approximated by cantilever beam theory, otherwise seagrasses exhibit a nonlinear whiplike motion, which cannot be approximated by using this theory (Zhu y Chen, 2015).

For the two L-associated conditions describe above, Luhar y Nepf (2011) defined equal

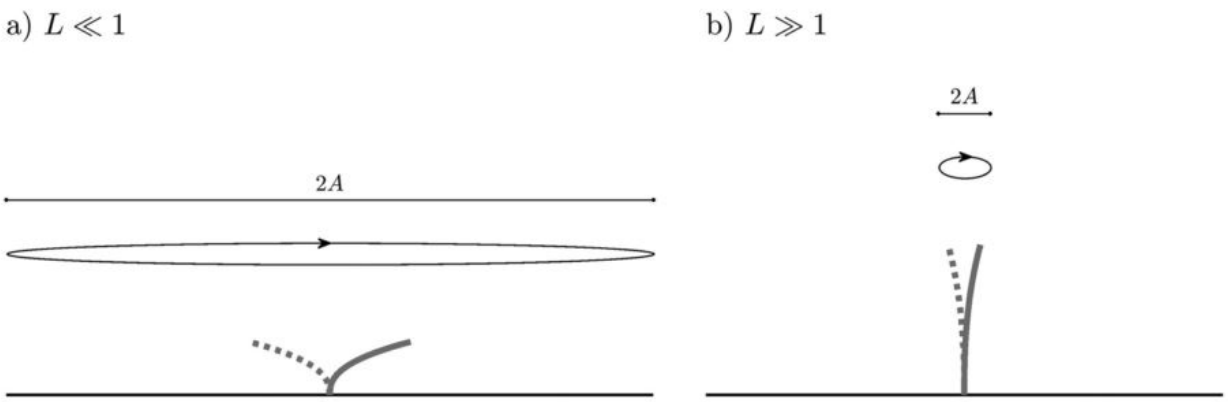

Figure 4.2: Plant movement in comparison with the oscillatory wave excursion (Luhar et al., 2016)

number of expressions to describe the equivalent lenght behaviour:

$$\frac{l_e}{h_v} \sim Ca^{-1/3}, \qquad L \ll 1,\ Ca \gg 1 \tag{4.9}$$

$$\frac{l_e}{h_v} \sim Ca\, L^{-1/4}, \qquad L \gg 1 \tag{4.10}$$

Additionally, Lei y Nepf (2019) considered the attenuation within the vegetation, changing the undisturbed velocity by the attenuated velocity through the inclusion of the velocity attenuation parameter (α_w), which was developed by Lowe et al. (2005) for rigid structures. However, attenuation parameter can be different between rigid and flexible conditions, assuming that flexibility is the only different parameter. As an example, the figure (4.3) presents the results of different experiments under the same wave conditions. The left panel plots the velocity profile of wave flow that interacts with rigid vegetation. The right panel shows the result for flexible vegetation. Note, the canopy density has significant effect on the velocity attenuation.
The experiments run by Luhar y Nepf (2016) showed that considering a wave excursion (A_∞) that is shorter than the inverse of vegetation frontal area per unit volume (a_v^{-1}), the assumption that fluid velocity over the entire water depth is given by linear wave theory is satisfied. But if A_∞ is much longer than a_v^{-1}, ($A_\infty a_v \ll 1$), in-canopy velocities are reduced significantly having a major impact on energy dissipation, which is proportional to U_∞^2 (Lowe et al., 2007) and the results are not accounted for in equation (4.2). Neglecting a significant diminishing of velocity within the meadow could produce a wave-energy attenuation 4 times greater than value obtained with flow attenuation accounted for (Lowe et al., 2007).

Considering equation (4.2) in an equivalent way (equation 4.11) by introducing the wave-

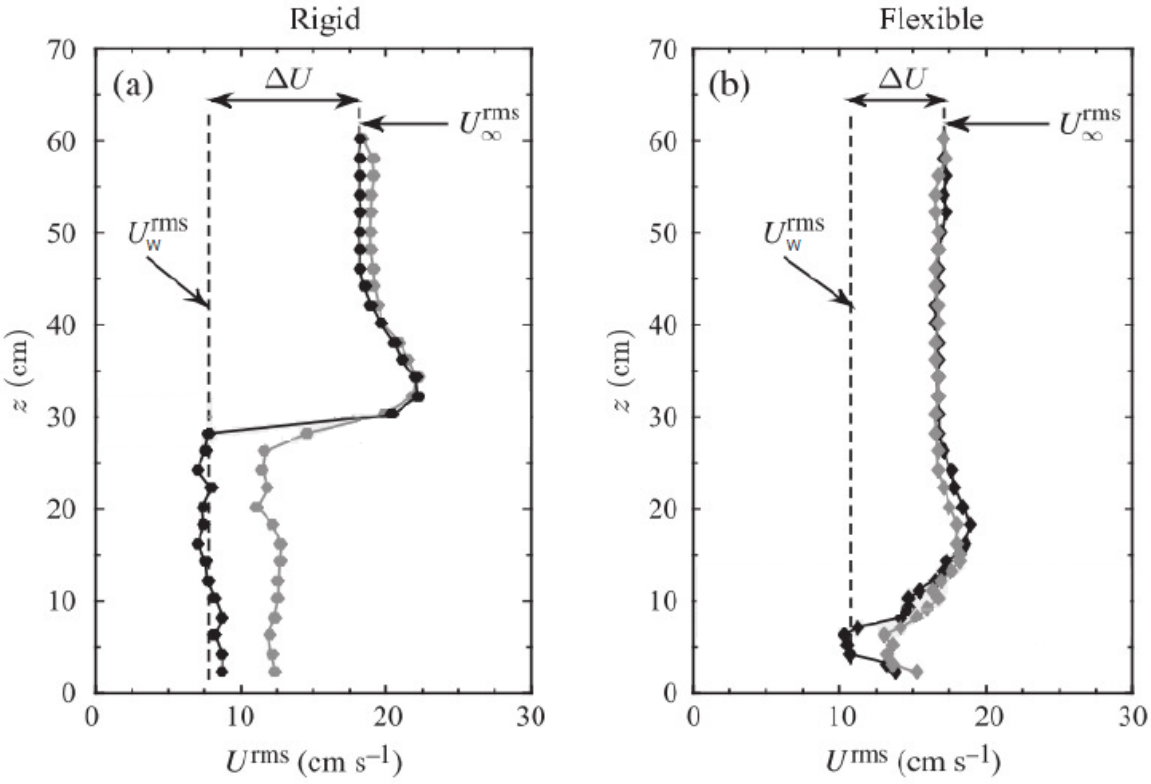

Figure 4.3: Velocity profiles of a flows that interact with rigid and flexible vegetation with different spatial densities, black and grey for high and medium density, respectively. Dashed lines are referred as references for the incident (U_∞^{rms}) and in-canopy (U_w^{rms}) velocities.

energy dissipation factor (f_e), which provides an estimate of the drag afforded by the seagrass meadow (Jonsson, 1966), it is possible to establish a relation between the rate of wave-energy dissipation and the canopy geometry parameters (height, width and spacing of the elements or spatial density of elements), the degree of flow attenuation (α_w), as well as coefficients that parameterise the effects of various forces exerted by the canopy elements, such as drag (C_D) and shear stress (C_f), (Lowe et al., 2007):

$$\varepsilon_v = \frac{2}{3\pi}\rho f_e (U_\infty^{max})^3 \tag{4.11}$$

$$f_e = C_f + C_D \lambda_f \alpha_w^3 \tag{4.12}$$

$$\alpha_w = \frac{\hat{U}_w^{rms}}{U_\infty^{rms}} \tag{4.13}$$

where λ_f is a parameter defined by the ratio of the canopy element frontal area to the underlying surface area (total area divided by the number of elements), α_w provides a quantitative measure of the reduction of the in-canopy velocity ($\hat{U}_w$) from its above-canopy potential flow value (U_∞). Here, the operator ($\hat{}$) signifies the vertical integrated value of a given variable integrated over the canopy height (from $z = 0$ to $z = h_v$) and divided by h_v. The factor f_e is narrowly related with the wave friction factor (f_w) that is vastly integrated on numerical models of near-shore wave propagation (e.g., SWAN or XBeach). Both are different according to their definitions. However, experimental estimations showed they can be assumed equal for practical purposes (Nielsen, 1992). For a intense description and calculation of f_w, Mirfenderesk y Young (2003) compiled expressions for the friction factor suggested by different authors. Extensive literature exists to relate f_w with the length scales of roughness (e.g., Nikuradse's equivalent sand grain roughness) (Mirfenderesk y Young, 2003; Pedocchi y Garcia, 2009). Nevertheless,the physical meaning of this variable is not clear for vegetated sea beds, excluding their application on these surfaces (Bradley y Houser, 2009).

To study wave-energy dissipation in a more extended case ($A_\infty a_v \gg 1$), attenuation of in-canopy velocity has to be considered. Lowe et al. (2005) developed a model considering the momentum balance around individual rigid canopy elements within a larger canopy in order to predict the in-canopy velocity ($\hat{U}_w$) and consequently, through equations (4.11 - 4.13) estimate the wave-energy dissipation. This model was employed not only for rigid canopy elements (i.e. corals) but also for flexible elements (i.e. seagrasses) (Luhar et al., 2010), including plant flexibility effects on the drag coefficient.

As a complementary approach, this study aims to improve the understanding of the effect of vegetation movement on estimation of in-canopy velocity attenuation and thus, the changes in drag coefficient. This approach exhibits a coupled model of vegetation motion (cantilever) and the momentum-balance model developed by Lowe et al. (2005).While these simple models do not capture the full complexity of a real seagrass, they are used in this study to obtain a better understanding of the flow attenuation by submerged vegetation.

4.2. Model for rigid vegetation

For a oscillatory flow due to progressive waves, it is well known that the instantaneous velocity (U_i), is the sum of steady velocity (U_c), pure wave motion (U), and turbulent velocity

(U'). For the horizontal component in the streamwise x direction, this relation is denoted as:

$$U_i = U_c + U + U' \tag{4.14}$$

when surface waves propagate over submerged vegetation, above the top of the canopy the oscillatory velocity field (U), is assumed to be undisturbed. Then, it is described by linear wave theory and denoted as (U_∞). Thus, the model assumes that U_∞ is independent of elevation z, which could be an acceptable approximation for shallow wave conditions. Under nonshallow wave conditions a minimal variation of U_∞ is required along the vertical axis, which is satisfied when the height of the vegetation is much smaller than the wavelength ($kh_v << 1$) Lowe et al., 2005. For the in-canopy velocity, U becomes U_w as was mentioned before.

$$U_\infty = U_\infty^{max} \cos \omega t \tag{4.15}$$

The momentum equation governing U in the horizontal x direction, which is valid for both within and above the canopy, is (Lowe et al., 2005; Lowe et al., 2007; Luhar et al., 2010; Trowbridge y Madsen, 1984):

$$\frac{\mathrm{D}U}{\mathrm{D}t} = -\frac{\partial}{\partial x}\frac{P_w}{\rho} + \frac{\partial}{\partial z}\frac{\tau_w}{\rho} - f_v \tag{4.16}$$

where $\mathrm{D}/\mathrm{D}t = \partial/\partial t + U\,(\partial/\partial x)$, P_w is pressure, τ_w is the shear stress and f_v is the canopy resistance term resulting from the force per unit fluid mass inside the canopy that is exerted on the flow by the canopy elements. The convective acceleration is neglected ($\partial/\partial x$) considering the relation ($kh_v \ll 1$). Accordingly, Trowbridge y Madsen (1984) showed that the ratio of the convective acceleration to local acceleration is small for for wave conditions $kA_\infty \sim \mathcal{O}(0.01)$, similar to the experiments employed in this study. Above the canopy top, the flow is unaffected by the shear stress and the resistance forces, and therefore oscillatory pressure gradient could be denoted as $(-1/\rho)\,\partial P_w/\partial x = \partial U_\infty/\partial t$. Under these considerations, equation (4.16) is stated as:

$$\frac{\partial U_w}{\partial t} = \frac{\partial U_\infty}{\partial t} + \frac{\partial}{\partial z}\frac{\tau_w}{\rho} - f_v \tag{4.17}$$

The external force f_v is expanded in two different terms, which include the drag (f_d) and inertia (f_i) forces. Now, equation (4.17) is vertically averaged from $z = 0$ to $z = h_v$ aiming to achieve an expression for $\hat{U}_w$:

$$\frac{\partial \hat{U}_w}{\partial t} = \frac{\partial U_\infty}{\partial t} + \frac{1}{h_v}\,\frac{\tau_w}{\rho}\bigg|_{z=0}^{z=h_v} - \hat{f}_d - \hat{f}_i \tag{4.18}$$

It is assumed that the stress at the base of the seagrass is negligible. At the top of the canopy the estresses can be parameterised using the velocity U_∞ (equivalent to the near-bed orbital velocity) considering only Reynolds stresses due to turbulence and assuming viscous stresses are negligible (Trowbridge y Madsen, 1984):

$$\tau_w(z = h_v) = \frac{1}{2}\rho\, C_f\, |U_\infty|\, U_\infty \tag{4.19}$$

where C_f is an empirical friction coefficient calculated under unidirectional flow conditions. C_f is generally two orders of magnitude smaller than C_D. The factor $2h_v/C_f$ is defined as L_s, which is a canopy shear length scale. The drag and inertia forces are represented as a Morison-type equation. Drag is considered a body force per unit volume on the spatially averaged flow and can be related to the drag of a typical and individual canopy element. The force exerted by the N elements at height z on water flow is $1/2\, C_d\, |U_w|\, U_w\, N\, b_v\, dz$ and the unit volume is defined as $(1 - \lambda_p)\, A_T\, dz$, where λ_p is the fractional volume occupied by the vegetation in the canopy and A_T is total plan area (fig. 4.4). In this case C_d is the so-called sectional drag coefficient, which depends on the vertical velocity profile. Considering a vertically averaged velocity ($\hat{U}_w$), C_d is assumed as the so-called depth-integrated drag coefficient, $C_D \sim 1/2\, C_d$ (Coceal y Belcher, 2004; Lowe et al., 2005). Finally, defining $a_v = N\, b_v/A_T$ and expression for canopy drag is established:

$$\hat{f}_d = \frac{C_D\, a_v}{1 - \lambda_p}\left|\hat{U}_w\right|\hat{U}_w \tag{4.20}$$

Now, we can define the drag length scale (L_d) that provides an indication of the strength of drag force exerted by the canopy:

$$\hat{f}_d = \frac{\left|\hat{U}_w\right|\hat{U}_w}{L_d} \tag{4.21}$$

Accordingly, at height z the inertia force is estimated as $C_M \lambda_p\, A_T\, dz\, \partial \hat{U}_w/\partial t$ where C_M is the inertia coefficient. As we mention before the unit volume is defined as $(1 - \lambda_p)\, A_T\, dz$, resulting in a total inertia force per unit volume equal to:

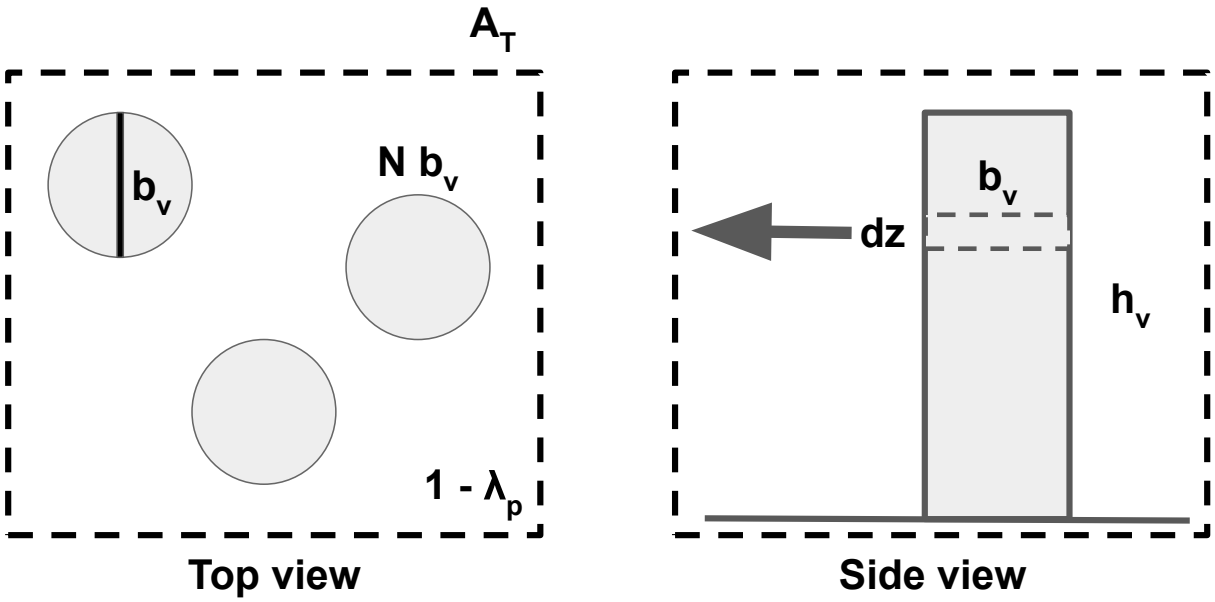

Figure 4.4: Schematic representation of submerged vegetation in a unit volume

$$\hat{f}_i = \left(\frac{C_M\,\lambda_p}{1-\lambda_p}\right)\frac{\partial \hat{U}_w}{\partial t} \tag{4.22}$$

Considering the previous equations for the shear stress, the drag and inertia forces, we achieve the following form of the equation (4.16) (Lowe et al., 2005):

$$\frac{\partial \hat{U}_w}{\partial t} = \frac{\partial U_\infty}{\partial t} + \frac{|U_\infty|\,U_\infty}{L_s} - \frac{\left|\hat{U}_w\right|\hat{U}_w}{L_d} - \left(\frac{C_M\lambda_p}{1-\lambda_p}\right)\frac{\partial \hat{U}_w}{\partial t} \tag{4.23}$$

5 Model development

5.1. Governing Equation of the Plant Motion

The behaviour of a seagrass meadow responds to both wave action and vegetation properties. Small wave perturbations generate vibrations in the seagrass blades. As wave action increases, seagrass blades become more flexible reaching a whip-like motion. While vibration and small displacements of vegetation take place, vegetation movements can be treated as a horizontal swaying. As long as the vegetation motion is not too large, it may be simply modelled as a forced vibration with one degree of freedom (Asano et al., 1992). As an approach, vegetation motion is modelled by a harmonic oscillation with respect to its vertical axis and no interaction between neighbouring plants as well. The governing equation of the plant motion is given by the balance between imposed loads and restoring forces, according to the Euler-Bernoulli beam equation for a cantilever beam with constant width and thickness (Asano et al., 1992; Dupont et al., 2010; Ikeda et al., 2001; Méndez y Losada, 1999; Maza et al., 2013):

$$\overbrace{\rho_v b_v t_v \ddot{\xi}}^{\text{Inertia}} + \overbrace{C_1 \dot{\xi}}^{\text{Damping}} + \overbrace{EI\xi^{(4)}}^{\text{Stiffness}} + \overbrace{(\rho - \rho_v)\, g b_v t_v \xi^{(1)}}^{\text{Buoyancy}} = \underbrace{\frac{1}{2}\rho\, C_D b_v \left|U_w - \dot{\xi}\right| \left(U_w - \dot{\xi}\right)}_{\text{Drag}} + \underbrace{\rho\, b_v\, t_v \left[C_M\, U_w - (C_M - 1)\ddot{\xi}\right]}_{\text{Inertia}} \quad (5.1)$$

where ρ_v is the blade density, ξ is the plant motion for any particular depth from $z = 0$ at the seabed to $z = h_v$ at the plant top, denoting $\partial/\partial t = (\dot{})$ and $\partial^{(i)}/\partial z^{(i)} = (\,)^{(i)}$ the derivatives are defined, and C_1 is a damping coefficient. Previous studies as Asano et al. (1992) and Méndez y Losada (1999) assumed $C_1 = 0$, however, Ikeda et al. (2001) y Maza et al. (2013) found a value of $C_1 \sim 12\, Nsm^{-1}$. The damping coefficient is related with blade geometrical properties and blade stiffness (Dupont et al., 2010). The seagrass used in this study differ mainly from blade thickness and modulus of elasticity reported by Ikeda et al. (2001) y Maza et al. (2013). Regardless of this difference a $C_1 = 12\, Nsm^{-1}$ was selected to be implemented. The terms on the left-hand side of equation (5.1) represent, the inertia, damping, stiffness, and gravity forces, respectively. The terms on the right-hand side are the drag and mass forces, respectively, which are modelled as a modified Morison type equation including the

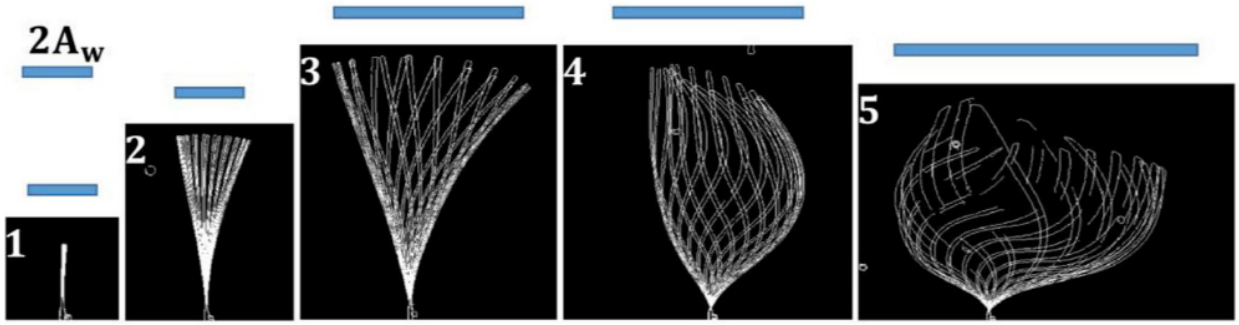

Figure 5.1: Types of plant movements

relative velocity and the added mass (Laya et al., 1984). Equation (5.1) assumes that the vertical force component is negligible compared to the horizontal component.

The movement described by equation (5.1) can be approximated by the horizontal displacement at the top of the vegetation (ζ), assuming that: i) the plant deformation is represented by a function varying linearly of z, $\xi = \zeta z/h_v$, and ii) that linear theory is valid. Considering these hypotheses and vertically integrating, equation (5.1) takes the form:

$$\frac{1}{2}\left[\rho\left(C_M - 1\right) + \rho_v\right] V_v \ddot{\zeta} + \left(\frac{1}{2}\rho\, C_D\, \hat{U}_w\, b_v\, h_c + C_1/2\right) \dot{\zeta} + \left[\frac{8EI}{h_v^3} + (\rho - \rho_v) g b_v t_v\right] \zeta = \frac{1}{2}\rho\, C_D b_v h_v \left|\hat{U}_w\right| \hat{U}_w + \rho\, C_M\, V_v \frac{\partial \hat{U}_w}{\partial t} \quad (5.2)$$

Equation (5.24) assumes $\dot{\zeta} \ll \hat{U}_w$, that is an acceptable assumption under the flow conditions and vegetation features considered in this study. Additionally, the vertical integration of the third term of the left hand side is assumed as the relation for the displacement at the top of a blade under uniform loading (Asano et al., 1992; Méndez y Losada, 1999):

$$\int_0^{h_v} EI\xi^{(4)}\, dz = \frac{8EI}{h_v^3}\zeta \quad (5.3)$$

5.2. The relative velocity

Studying of the response of seagrasses to wave action, i.e. drag and inertia forces, is frequently done through an empirical Morison's equation. However, this equation was initially developed to estimate wave loading on rigid structures (Morison et al., 1950). When flexible structures are considered, a modified model of the Morison's equation needs to be introduced. Typically, two approaches are used: (i) the relative-velocity form and (ii) the independent-flow form

of Morison's equation. The first one is the most commonly used assuming that the drag force is proportional to the square of relative velocity defined as $U_r = U_w - \dot{\xi}$. In the second approach, the drag force is the sum of the wave force by acting on a fixed structure and the force due to the structure vibration assuming still water conditions (Chakrabarti, 1987; Laya et al., 1984; Yuan y Huang, 2015). Laya et al. (1984) established limits for the application of both forms based on the Keulegan–Carpenter number (KC) and the so-called reduced velocity (V_R):

$$KC = \frac{U_\infty^{max} T}{b_v} = \frac{\sqrt{8}\pi A_\infty^{rms}}{b_v} \tag{5.4}$$

$$V_R = \frac{U_\infty^{max} T_v}{b_v} \tag{5.5}$$

where the superindexes max and rms are the maximum value and the root-mean-square operator, respectively. A_∞ represents the wave excursion and T_v is the oscillatory plant period. In general, relative-velocity form requires $KC > 10 - 15$ and $V_R > 10 - 15$ to be applicable. On the other hand, independent-flow form takes relevance for small values of KC and V_R. Additionally, when a significant variation in oscillatory frequencies of flow and structure is presented, erratic flow patterns occur near the structure vicinity and the relative-velocity form is highly suspected (Chakrabarti, 1987; Laya et al., 1984; Yuan y Huang, 2015). Even thought, seagrasses exhibit an oscillatory movement with similar period to wave period ($T_v = T$) so that it is not an independent motion (e.g., Zhu y Chen (2015)). For this particular study, $KC > 38$, indicating that the relative-velocity form of Morison equation can be employed to described the interaction between oscillatory flow and seagrasses.

To include the relative velocity into the approach developed by Lowe et al. (2005), it has to be vertically averaged to establish an equation governing the in-canopy velocity with deformable vegetation:

$$\hat{U}_r = \frac{1}{h_v} \int_0^{h_v} \left(U_w - \frac{\partial \xi}{\partial t} \right) dz \tag{5.6}$$

Assuming the vegetation is moderately flexible and the cantilever beam theory applies to describe the plan movement, the relation ($\xi = \zeta z / h_c$) is considered to model the horizontal displacement as a function of the horizontal displacement at the top of the vegetation blade. The displacement at the top of the blade is independent of the z coordinate, allowing it can be considered as a constant with respect to z:

$$\begin{aligned}\hat{U}_r &= \frac{1}{h_v}\int_0^{h_v}\left(U_w - \frac{z}{h_v}\frac{\partial\zeta}{\partial t}\right)dz \\ &= \hat{U}_w - \frac{\partial\zeta}{\partial t}\frac{1}{h_v^2}\int_0^{h_v} z\,dz \\ &= \hat{U}_w - \frac{1}{2}\frac{\partial\zeta}{\partial t}\end{aligned} \tag{5.7}$$

As long as vegetation motion becomes important to in-canopy velocity attenuation, the forcing terms, based on Morison's equation, must be modified for predicting the forces exerted by vegetation. The seagrasses feature as deformable vegetation, which respond to water flow stresses and reciprocally, alter the surrounded hydrodynamics. As a consequence, the drag force exerted by the canopy is proportional to the relative velocity. In addition, drag is modified due to the frontal area of the seagrass that is reduced when the elements begin to sway (Bradley y Houser, 2009). On the other hand, the inertia force contains an added mass term proportional to the vegetation acceleration, which considers the surrounded water that moves with the vegetation (Laya et al., 1984). Denoting $\partial\zeta/\partial t = \dot{\zeta}$, the forcing terms can be redefined as :

$$\hat{f}_v = \frac{\left|\hat{U}_w - \dot{\zeta}/2\right|\left(\hat{U}_w - \dot{\zeta}/2\right)}{L_d} + \left(\frac{\lambda_p}{1-\lambda_p}\right)\left[C_M\frac{\partial\hat{U}_w}{\partial t} - \left(\frac{C_M-1}{2}\right)\ddot{\zeta}\right] \tag{5.8}$$

Finally, here we presented the developed model to estimate the in-canopy velocity considering rigid or moderately flexible submerged vegetation:

$$\frac{\partial\hat{U}_w}{\partial t} = \frac{\partial U_\infty}{\partial t} + \frac{|U_\infty|\,U_\infty}{L_s} - \frac{\left|\hat{U}_w - \dot{\zeta}/2\right|\left(\hat{U}_w - \dot{\zeta}/2\right)}{L_d} - \left(\frac{\lambda_p}{1-\lambda_p}\right)\left[C_M\frac{\partial\hat{U}_w}{\partial t} - \left(\frac{C_M-1}{2}\right)\ddot{\zeta}\right] \tag{5.9}$$

5.2.1. Dimensionless Model

To determine the relative magnitude of each term in equation (5.9), a scaling analysis was performed. The model was nondimensionalised by using characteristic velocities, displacement and time. The velocities U_∞ and $\hat{U}_w$ were scaled by the root-mean-squared incident velocity U_∞^{rms}, ζ by $2A_\infty^{rms}$, and time was scaled by ω^{-1}. The dimensionless variables were denoted by the superscript (*).

$$\hat{U}_w^* = \frac{\hat{U}_w}{U_\infty^{rms}}; \qquad U_\infty^* = \frac{U_\infty}{U_\infty^{rms}}; \qquad \zeta^* = \frac{\zeta}{2A_\infty^{rms}}; \qquad t^* = \omega t \tag{5.10}$$

Including equations (5.10) into (5.9) and and rearranging gives:

$$\frac{\partial\left(\hat{U}_w^* - U_\infty^*\right)}{\partial t} = A_\infty^{rms}\left[\frac{|U_\infty^*|\,U_\infty^*}{L_s} - \frac{\left|\hat{U}_w^* - \dot{\zeta}^*\right|\left(\hat{U}_w^* - \dot{\zeta}^*\right)}{L_d}\right] - \left(\frac{\lambda_p}{1-\lambda_p}\right)\left[C_M\frac{\partial\hat{U}_w^*}{\partial t} - (C_M - 1)\,\ddot{\zeta}^*\right] \tag{5.11}$$

From equation (5.19), it is visible that if the wave excursion is smaller than the shear length scale ($A_\infty^{rms} \ll L_s$) the wave motion is unaffected by the shear stress, and the flow is dominated by the other terms (Lowe et al., 2005; Luhar et al., 2010). For the experiments considered in this study and assuming a constant $C_f = 0{,}05$ (Ghisalberti y Nepf, 2006), $A_\infty^{rms} \sim 1{,}5\,m$ whereas $L_s \sim 5 - 10\,m$. It is inferred then, that the shear stress has a small effect on the in-canopy velocity attenuation. The drag term depends on A_∞^{rms}/L_d and the plant stiffness, which implicitly affects the plant velocity and subsequently, the relative velocity. For instance, for an extremely rigid vegetation, the plant velocity can be neglected ($\dot{\zeta}^* \to 0$), whereas for extremely flexible vegetation, the plant follows the movement of the surrounding water particles ($\dot{\zeta}^* \to 2\hat{U}_\infty^*$), reducing significantly the drag force. For the inertia-dominated regime, where $A_\infty^{rms} \ll L_s$ and $A_\infty^{rms} \ll L_d$, but the inertia parameters $(C_M\lambda_p)/(1-\lambda_p)$ and $(C_M - 1)\lambda_p/(1-\lambda_p)$ are not negligible, the canopy inertia and added mass forces are expected to contribute most to the attenuation of the oscillatory canopy flow (Lowe et al., 2005). Neglecting the shear and the drag force terms of the equation (5.19), it is possible to establish a new equation for the in-canopy velocity under the inertia-dominated regime:

$$\frac{\partial\hat{U}_w^*}{\partial t^*} = \frac{U_\infty^*}{\partial t^*} - \left(\frac{\lambda_p}{1-\lambda_p}\right)\left[C_M\frac{\partial\hat{U}_w^*}{\partial t} - (C_M - 1)\,\ddot{\zeta}^*\right] \tag{5.12}$$

There are two cases that can be easily calculated. For stiff vegetation, ($\ddot{\zeta}^* \to 0$), and for extremely flexible vegetation, ($\ddot{\zeta}^* \to \partial\hat{U}_\infty^*/\partial t^*$). Considering the first case we achieve the following equation:

$$\frac{\partial\hat{U}_w^*}{\partial t^*} = \frac{U_\infty^*}{\partial t^*} - \left(\frac{C_M\,\lambda_p}{1-\lambda_p}\right)\frac{\partial\hat{U}_w^*}{\partial t} \tag{5.13}$$

Now, we reorganise the terms leaving the local acceleration ($\partial\hat{U}_w^*/\partial t^*$) on the left hand side:

$$\frac{\partial\hat{U}_w^*}{\partial t^*} = \frac{1-\lambda_p}{1+(C_M-1)\lambda_p}\frac{\partial\hat{U}_\infty^*}{\partial t^*} \tag{5.14}$$

Then, we take the root-mean-square (rms) operator on the both sides of the last equation and considering the velocities and accelerations are sinusoidal functions with proportional amplitudes, the limiting value of α_w for inertia-dominated regime is obtained:

$$\alpha_i = \frac{1-\lambda_p}{1+(C_M-1)\lambda_p} \tag{5.15}$$

When this last expression is analysed it can be seen it is exactly the same as in Lowe et al. (2005), which considers the movement of the occupied water fraction $(1-\lambda_p)$. Continuing with the second case, we assumed $\ddot{\zeta}^* \approx \partial\hat{U}_w^*/\partial t^*$:

$$\frac{\partial\hat{U}_w^*}{\partial t^*} = \frac{U_\infty^*}{\partial t^*} - \left(\frac{\lambda_p}{1-\lambda_p}\right)\frac{\partial\hat{U}_w^*}{\partial t} \tag{5.16}$$

Reorganising:

$$\frac{\partial\hat{U}_w^*}{\partial t^*} = \left(\frac{1}{1+(C_M-1)\lambda_p}\right)\frac{\partial\hat{U}_\infty^*}{\partial t^*} \tag{5.17}$$

Furthermore, taking the rms operator:

$$\alpha_i = \frac{1}{1+(C_M-1)\lambda_p} \tag{5.18}$$

5.2.2. Numerical Solution

As first step to estimate the in-canopy velocity, equation (5.19), which is presented here again:

$$\frac{\partial\left(\hat{U}_w^* - U_\infty^*\right)}{\partial t} = A_\infty^{rms}\left[\frac{|U_\infty^*|\,U_\infty^*}{L_s} - \frac{\left|\hat{U}_w^* - \dot{\zeta}^*\right|\left(\hat{U}_w^* - \dot{\zeta}^*\right)}{L_d}\right] - \left(\frac{\lambda_p}{1-\lambda_p}\right)\left[C_M\frac{\partial\hat{U}_w^*}{\partial t} - (C_M - 1)\,\ddot{\zeta}^*\right] \quad (5.19)$$

This equation is discretised by employing an explicit scheme and linearised by staggering the step numbers on the quadratic nonlinear terms of plant and flow velocities, following the procedure described by Lowe et al. (2005). Previously, some parameters are defined to simplify the notation:

$$A = \frac{A_\infty^{rms}}{L_s}, \quad B = \frac{A_\infty^{rms}}{L_d}, \quad C = \frac{C_M\lambda_p}{1-\lambda_p}, \quad C' = C\frac{(C_M - 1)}{C_M} \quad (5.20)$$

Equation (5.19) can be rewritten as:

$$(1+C)\,\frac{\partial\hat{U}_w^*}{\partial t^*} = A\;|U_\infty^*|\,U_\infty^* - B\left|\hat{U}_w^* - \dot{\zeta}^*\right|\left(\hat{U}_w^* - \dot{\zeta}^*\right) + C'\ddot{\zeta}^* + \frac{\partial U_\infty^*}{\partial t^*} \quad (5.21)$$

Now, equation (5.21) is discretised and linearised:

$$\hat{U}_w^{*(i+1)} = \frac{1}{D}\left[A\left|U_\infty^{*(i)}\right|U_\infty^{*(i+1)} + B\left|\hat{U}_w^{*(i)} - \dot{\zeta}^{*(i)}\right|\dot{\zeta}^{*(i+1)} + C'\frac{\Delta\dot{\zeta}^{*(i)}}{\Delta t^{*(i)}} + \frac{\Delta U_\infty^{*(i)}}{\Delta t^{*(i)}} + \frac{1+C}{\Delta t^{*(i)}}\,\hat{U}_w^{*(i)}\right] \quad (5.22)$$

where

$$D = \frac{1+C}{\Delta t^*} + B\left|\hat{U}_w^{*(i)} - \dot{\zeta}^{*(i)}\right| \quad (5.23)$$

and $\Delta(\;)^{(i)} = (\;)^{(i+1)} - (\;)^{(i)}$.

Second, remembering the dimensional governing equation of the plant movement (5.1):

$$\frac{1}{2}\left[\rho\left(C_M-1\right)+\rho_v\right]V_v\ddot{\zeta}+\left(\frac{1}{2}\rho\,C_D\,\hat{U}_w\,b_v\,h_c+C_1/2\right)\dot{\zeta}+\left[\frac{8EI}{h_v^3}+(\rho-\rho_v)gb_vt_v\right]\zeta$$
$$=\frac{1}{2}\rho\,C_Db_vh_v\left|\hat{U}_w\right|\hat{U}_w+\rho\,C_M\,V_v\,\frac{\partial\hat{U}_w}{\partial t} \quad (5.24)$$

We nondimensionalise it and consider the following notation for simplicity:

$$a=\frac{1}{2}\left[\rho\left(C_M-1\right)+\rho_v\right]V_v,\quad b=\left[\frac{8EI}{h_v^3}+(\rho-\rho_v)gb_vt_v\right] \quad (5.25)$$

$$\ddot{\zeta}^*+\frac{1}{a}\left(\frac{1}{2}\rho\,C_D\,A_\infty^{rms}\hat{U}_w^*\,b_v\,h_v+\frac{C_1}{2\omega}\right)\dot{\zeta}^*+\left(\frac{b}{2\,a\,\omega^2}\right)\zeta^*$$
$$=\frac{1}{2a}\left(\frac{1}{2}\rho\,C_Db_vh_vA_\infty^{rms}\left|\hat{U}_w^*\right|\hat{U}_w^*+\rho\,C_M\,V_v\,\frac{\partial\hat{U}_w^*}{\partial t}\right) \quad (5.26)$$

Notice equation (5.26) is a linear second order differential equation. This was solved employing the Python-based open-source routine `odeint` from the software SciPy.

The dimensionless forcing term or above-canopy velocity is estimated as $U_\infty^*=\sqrt{2}\cos\left(t^*\right)$. It is a result of assuming $U_\infty^{max}=\sqrt{2}\,U_\infty^{rms}$. Then, it is needed to achieve values for $\hat{U}_w^*$ and $\dot{\zeta}$. The figure (5.2) presents an scheme of the procedure employed to couple both flow and plant movement models. This scheme is divided in two dotted rectangles that symbolise the employed models, left for the equation (5.19) and right for (5.26), working within an i-th time step:

- Initially, considering that the plant velocity is unknown, temporally values are assumed to initialise the models as it is shown in the first row of the figure (5.2). Note in this particular case the models start from $U_w^{*(i+1)}$ and $\dot{\zeta}^{*(i)}$.

- Taking these assumptions, the movement and velocity of the plant are calculated in the step $(i+1)$.

- Employing the plant velocity in the steps (i) and $(i+1)$, and the in-canopy velocity in step (i), the in-canopy velocity in step $(i+1)$ is recalculated. At the beginning of the process this velocity is not well estimated, it is needed to iterate between the both models to reach a stable value of the flow and plant velocities. In this particular case, this iteration took just tree steps to converge.

- Now, it is possible to move in time updating the forcing therm U^*_∞ and for the next (i+1)-th step (grey solid lines). It is expected that initial conditions do not satisfy both models, it is needed to move forward in time at least a couple of wave cycles to models respond properly.

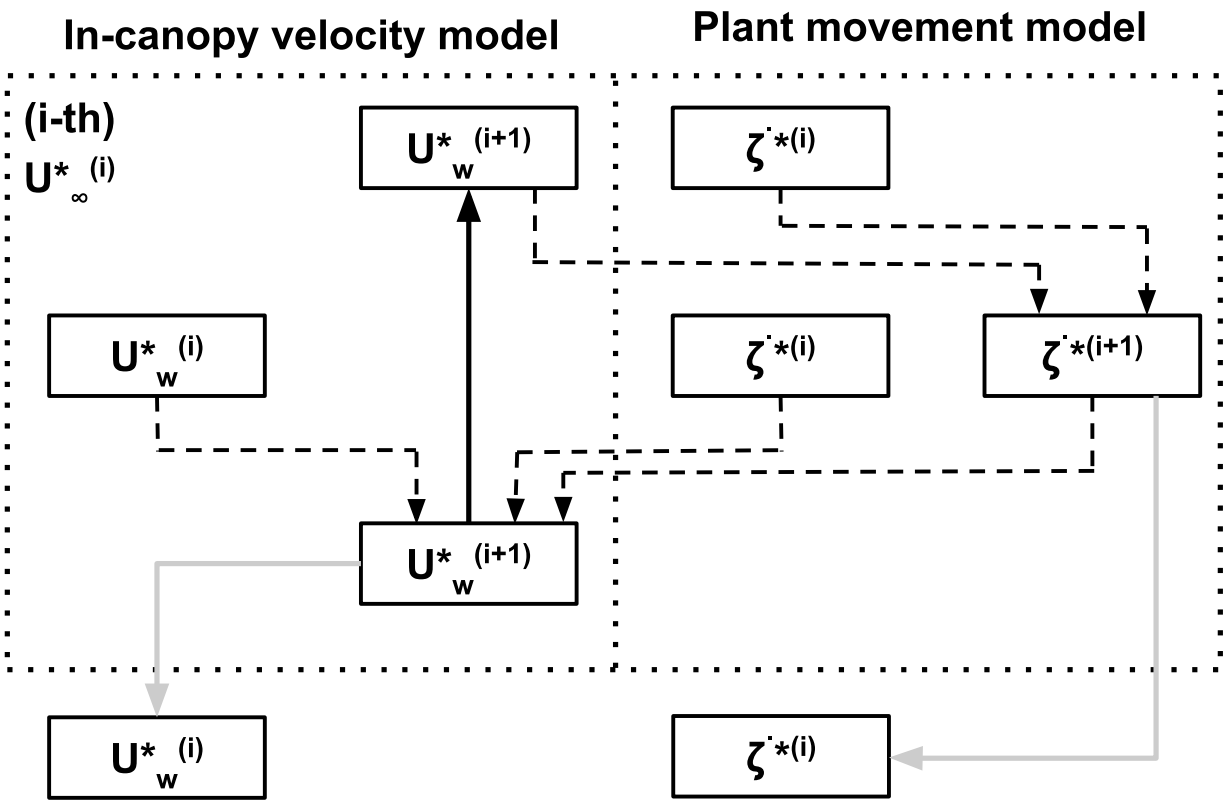

Figure 5.2: Scheme of the coupling to achieve the numerical solution. Dotted rectangles mean the models employed. Dashed arrows indicate the inputs and the output during the coupling. The solid arrow is the iterative process.

6 Data

To explore the performance of the developed model, the simulated results were compared with the artificial seagrass experiments conducted by Abdolahpour et al. (2018). The experiments included two types of submerged structures, rigid and flexible, with identical heights and frontal areas where flexibility was the only difference between both. Two canopy densities were considered i.e. medium and high, which alter the dimensionless frontal area ($a_v b_v$) and the solid fraction of vegetation (λ_p). For the flexible vegetation the dimensionless frontal area is based on the effective blade width ($a_v b_e$) due to the vertical variation of the blade width. The value b_e was taken as the vertically averaged width. Rigid model plants were made of birch dowels with height of $h_v = 30\,cm$, attached to perforated PVC boards. The flexible vegetation models correspond to the species *Posidonia australis* that consists of two blades with different height ($15\,cm$ and $30\,cm$). The figure (6.1) shows the experimental set up employed by this study.

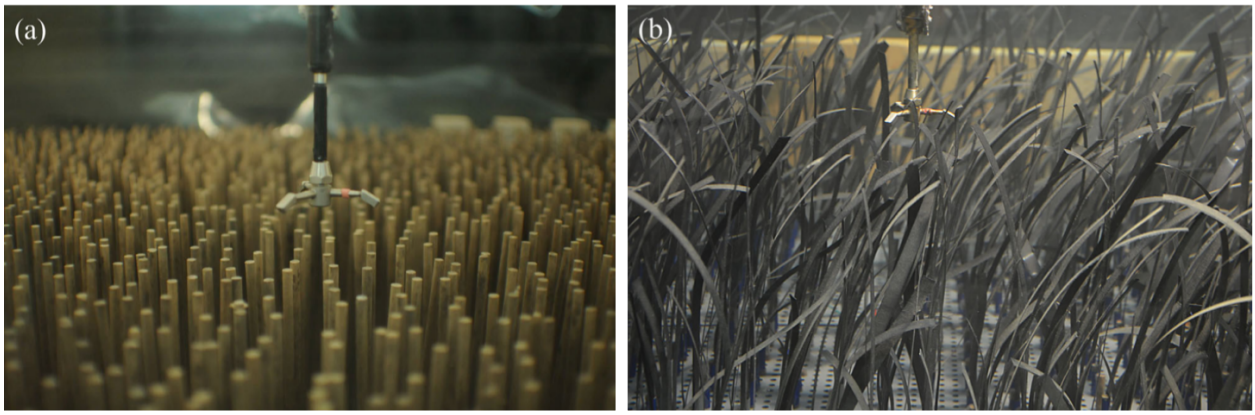

Figure 6.1: The experimental setup and the ADV probe, (a) rigid model of vegetation and (b) mimics of seagrass (Abdolahpour et al., 2017a).

To mimic the *Posidonia australis*, blades were made of Low Density Polyethylene, which resulted in an estimated blade thickness of $t_v = 0{,}3 \pm 0{,}06\,mm$, a seagrass density of $\rho_v = 860 \pm 78\,kg\,m^{-3}$, and a Young's modulus of $E = 0{,}4 - 2{,}4\,GPa$, based on similar values reported for *Zostera marina*. The table (6.1) shows the vegetation parameters including blade widths and canopy densities employed in this study.

Table 6.1: Blade width and canopy density

Vegetation type	$b_v, b_e\,(mm)$	**Density**	$a_v b_v, a_v b_e$	$L_d\,(m)$
Rigid	6.4	M (medium)	0.063	0.10
(R)		H (high)	0.131	0.05
Flexible	15	M (medium)	0.064	0.16
(F)		H (high)	0.145	0.07

The velocity records were taken by an Acoustic Doppler Velocimeter (ADV) in the centre of the canopy. For the rigid vegetation, data points were spaced every $2\,cm$; in flexible canopies, velocity data were measured every $1\,cm$ for $z < 16\,cm$, and every $2\,cm$ for $z \geq 16\,cm$. Data were recorded at $25\,Hz$ in all the velocity profiles. The sampling time was variable for rigid and flexible vegetation. For the first case, a 6 min (40–70 wave cycles) was employed, whereas for the second one this was increased to 10 min (70–120 wave cycles) to consider the removal of corrupted data due to seagrass blades contaminating the ADV signal entering the sampling volume. These removals did not significantly altered the velocity profiles demostrated by the convergence of flow statistics.

As was aforementioned, there are different kinds of vegetation movement from cantilever-like to whip-like motion depending of the parameter $Ca\,L$. Experiments run by Abdolahpour et al. (2018) range $10^{-1} < Ca\,L < 10^3$, which could be classified within groups 1-3 in the figure (5.1) (Lei y Nepf, 2019). Plant motion presented in group 3 and 4 corresponds to $Ca\,L > 3 \times 10^3$, which is not well represented by the developed model. The operative range were satisfied by the following flow conditions. Still water depth was kept constant for all experiments, $h = 76\,cm$; the wave period and the above-canopy rms velocity were varied, $T = 5 - 9\,s$ and $U_\infty^{rms} = 3{,}0 - 22\,cm\,s^{-1}$. These ranges allowed that experiments took place in shallow-water waves with $kh < 0{,}35$. Flow regimens resulted in $420 < Re < 3000$ and $38 < KC < 192$. Moreover, the product between Cauchy number and the blade length ratio ranges $5 \times 10^1 < Ca\,L < 6 \times 10^2$.

Rigid and flexible vegetation were exposed to an ensemble of 19 flow conditions by varying the wave period and the above-canopy rms velocity. The differences between above-canopy rms velocity and in-canopy rms velocity ($\Delta U = U_\infty^{rms} - U_w^{rms}$) and the parameter $Ca\,L$ associated to each experiment are presented in the table (6.2).

Table 6.2: Wave conditions and wave velocity reductions

Run	$\boldsymbol{T\,(s)}$	$\boldsymbol{U_\infty^{rms}}$	***Re***	***KC***	***Ca L***	$\boldsymbol{\Delta\, U\ (cm\, s^{-1})}$			
						RM	***RH***	***FM***	***FH***
1	5	15	2100	106	4×10^2	5.2	12.7	1.9	2.7
2	5	19	2660	134	6×10^2	9.5	12.6	3.8	3.5
3	6	8.2	1148	70	2×10^2	0.3	1.4	-	1.3
4	6	9.4	1316	80	2×10^2	2	2	1.1	2.8
5	6	16	2240	136	4×10^2	1.6	4.8	2.2	3.1
6	6	19	2660	161	5×10^2	7.5	13.6	3.8	3.8
7	6	22	3080	187	5×10^2	6.3	9.7	-	-
8	8	5.6	784	63	1×10^2	0.7	0.8	0.5	0.6
9	8	7.7	1078	87	1×10^2	1.6	4.6	1.2	1.4
10	8	9.8	1372	111	2×10^2	1.7	5.5	2	1.8
11	8	12	1680	136	2×10^2	3	9.4	2.6	4.3
12	8	15	2100	170	3×10^2	4.4	9.4	2.4	4
13	8	17	2380	192	3×10^2	7.2	15.7	2.9	5.3
14	9	3	420	38	5×10^1	1.2	0.4	-	-
15	9	4.4	616	56	7×10^1	-	1.1	0.4	0.4
16	9	5.9	826	75	1×10^2	1.2	2.9	-	1
17	9	7.5	1050	95	1×10^2	1.3	2.3	-	1.2
18	9	11	1540	140	2×10^2	2	6.4	1.8	2
19	9	12	1680	153	2×10^2	9.8	9.9	1.4	2.7

7 Results

7.1. Sensitivity of the model coefficients

Oscillatory flow experiments conducted by Lowe et al. (2005) were numerically replicated by using equation (4.23) to evaluate the performance of the model with rigid vegetation. A submerged cylinder array was exposed to 16 wave flow experiments. Cylinders feature a diameter of $b_v = 5\,cm$, a height of $h_v = 10\,cm$ and three relation uniform spacing to diameter $S_v/b_v = 1$, 2 and 3. The reported model coefficients were also used, $C_D = 1$, $C_M = 2$, and $C_f = 0{,}02$. Some slight differences were found between the previous and calculated attenuation coefficients (α_w). These can be explained by the fact that, in this study, we employed the reported values of U_∞^{rms} and wave period (T), exactly as table (7.1) shows instead of the exact value with better resolution used by Lowe et al. (2005). Regardless of these small discrepancies, we run a sensitivity analysis to identify the impact of C_f, C_D and C_M on in-canopy velocity attenuation coefficient (α_w).

Table 7.1: Parameters for the replicated wave experiments

Run	W1	W2	W3	W4	W5	W6	W7	W8	W9	W10	W11	W12	W13	W14	W15	W16
S_v/b_v	1	1	1	1	1	1	2	2	2	2	3	3	3	3	1	1
U_∞^{rms} $(cm\,s^{-1})$	2.4	4.8	3.5	2.0	3.1	2.2	2.3	5.2	3.4	3.7	2.5	5.3	3.4	3.2	3.8	3.6
$T\,(s)$	1	2	3	1	2	3	1	2	3	2	1	2	3	2	2	2
α_w*	0.66	0.66	0.66	0.66	0.66	0.66	0.83	0.83	0.83	0.83	0.90	0.90	0.90	0.90	0.66	0.66
α_w	0.67	0.67	0.67	0.67	0.67	0.67	0.84	0.83	0.83	0.83	0.90	0.90	0.90	0.90	0.67	0.67

* Reported by Lowe et al. (2005).

The drag (C_D) and inertia coefficients (C_M) are strongly dependant of Keulegan-Carpenter number (KC) and Reynolds number (Re). Méndez y Losada (1999) showed that the drag coefficient depends directly on the Reynolds number. However, more recently Mendez y Losada (2004) found that the drag coefficient is better represented as function of KC, allowing, for a given canopy, C_D decreasing as the wave excursion length A_∞ is increased (Lowe et al., 2007). To characterise the flow, three different flow regimes can be established according to KC, i.e., inertia ($KC < 7$), drag-inertia ($7 < KC < 20$) and drag dominated regime ($KC > 20$) (Etminan et al., 2019). Frequently, vegetation is assumed as groups of cylinders or rectangular plates (Méndez y Losada, 1999; Maza et al., 2013; Etminan et al., 2019). Keulegan y Carpenter (1958) run systematical experiments to estimate drag and

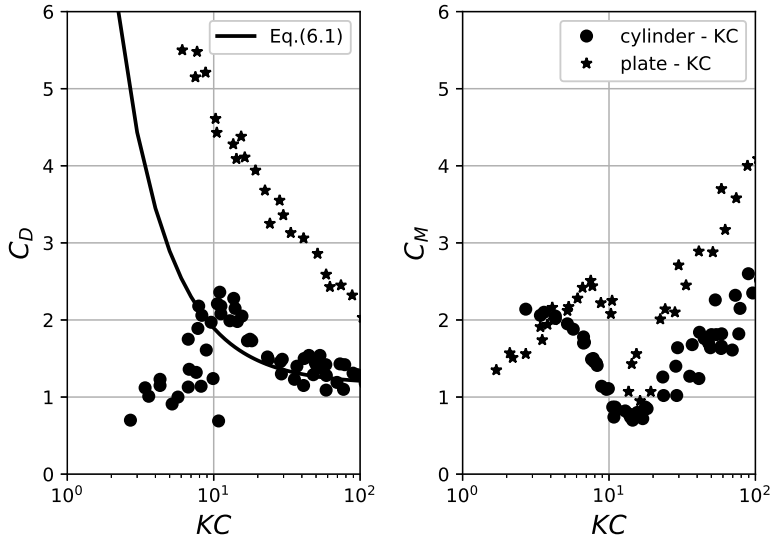

Figure 7.1: Drag and inertia coefficients employed in the sensitivity analysis. Circles and stars are drag coefficients for a single rigid cylinder and plate, respectively (Keulegan y Carpenter, 1958). The solid line is the equation reported by (Chen et al., 2018)

.

inertia coefficients for both single rigid cylinder and plate as function of KC. Their results are plotted on figure (7.1) as circles and stars for cylinder and plate, respectively. Additionally, Chen et al. (2018) presented a review of C_D relations in vegetation-wave interaction, either Reynolds- and Keulegan–Carpenter-based. They developed a reviewed formula to estimate C_D for rigid vegetation that fits Keulegan y Carpenter (1958) for $KC > 10$:

$$C_D = 12{,}89\, KC^{-1{,}25} + 1{,}17, \qquad R^2 = 0{,}66 \tag{7.1}$$

Under inertia dominated regime, variations of C_D diverge for single or cylinder array estimations ($\sim 0{,}6 - 4$). For a single plate, C_D can reach ~ 6 (Keulegan y Carpenter, 1958; Chen et al., 2018). However, it is noticed that under this regime C_D does not have an important effect on α_w, as figure (7.2) shows. In the drag-inertia and drag dominated regimes, drag coefficients are well estimated by the potential equation based on KC. For inertia dominated regime, in general, C_M is not significant affected by Re and values are only dependant of KC, although, for the two geometries considered in this study, C_M is bounded between $\sim 1{,}7 - 2{,}5$. In the drag-inertia dominated regime, C_M decreases to a minimum value ($C_M \sim 0{,}85$), corresponding to the conditions in which a single eddy is shed from the structures during each wave half-cycle (Keulegan y Carpenter, 1958; Luhar

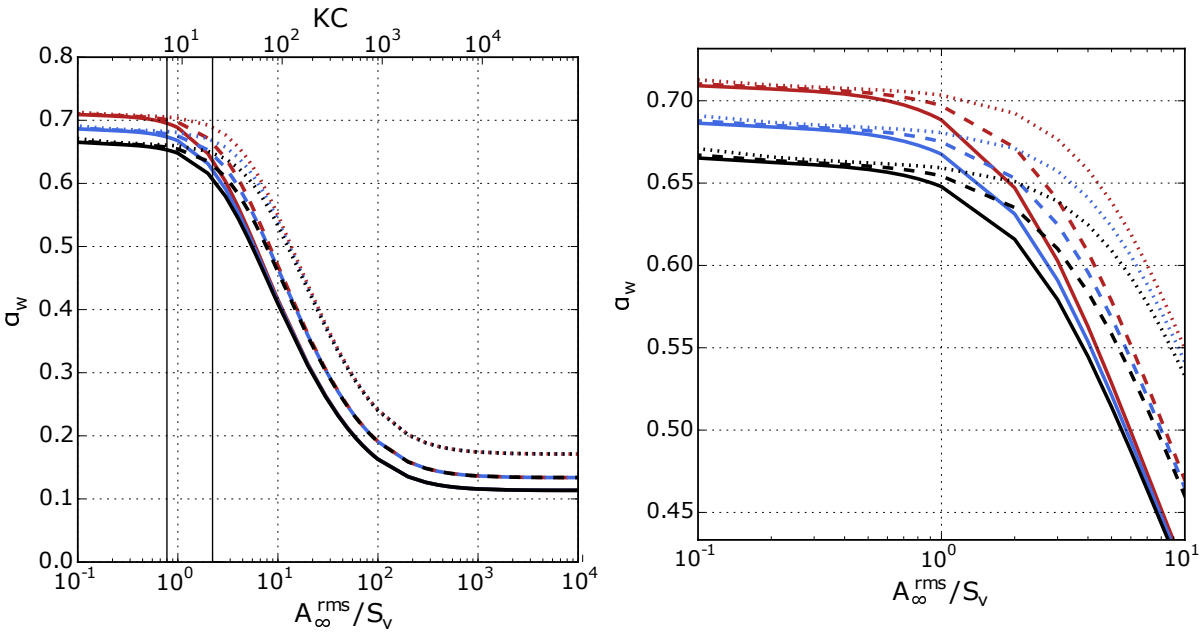

Figure 7.2: Attenuation coefficients for different wave conditions (A_∞^{rms}) and mean spacing between elements (S_v)

.

y Nepf, 2016). As the KC continues increasing (> 20), C_M becomes larger, however, drag force dominance grows rapidly limiting the inertia effect.

The empirical friction coefficient, (C_f), is used to parameterise the shear stress on the vegetation top. Previous studies of unidirectional flow over canopies have reported that $C_f \sim 0{,}01 - 0{,}08$ (Lowe et al., 2005; Luhar et al., 2010). It can vary as a function of both the roughness geometry and flow conditions (i.e., unidirectional or oscillatory flow) (Lowe et al., 2005). However, there is just a slight effect in the drag dominated regime. For simplicity, in this sensitivity analysis we assume a constant value, $C_f = 0{,}02$, which does not significantly alter the attenuation coefficients obtained for all the cases considered here.

Based on the analysis presented above, three drag and inertia coefficients were considered, $C_D = [1{,}1,\ 1{,}8,\ 2{,}5]$, and $C_M = [1{,}7,\ 1{,}9,\ 2{,}1]$. Considering a spacing to element width ratio, $S_v/b_v = 1$, the model described in section (4.2) was run for different A_∞^{rms}/S_v conditions and results are presented in figure (7.2). Each inertia coefficient was assigned a colour, light grey, grey and black, respectively to the C_M list. Furthermore, line type was selected considering different drag coefficients, dotted, dashed and solid lines, respectively to the C_D list. For all the considered A_∞^{rms}/S_v range, the variation of the attenuation coefficient is less than 10 %. For the inertia-drag regimen flow a different combinations of C_M and C_D can lead to the same attenuation coefficient.

From the figure (7.2), it can be seen the more significant reduction in the attenuation coefficient occurs when $A_\infty^{rms}/S_v > 10$. Considering that for this analysis $S_v/b_v = 1$, the KC number can be denote in terms of S_v as $KC = \sqrt{8}\,\pi A_\infty^{rms}/S_v$ where $\sqrt{8}\,\pi \sim 9$. In this sense, the KC could be plotted on the figure (7.2).

7.2. In-canopy velocity attenuation by rigid vegetation

The model developed by Lowe et al. (2005) could be considered to analyse in-canopy velocity attenuation when rigid structures are place on the bottom. Employing this model, the experiments conducted by Abdolahpour et al. (2018) were numerically simulated. As inputs, the parameters described in the table (6.1) were taken into account to establish the geometric features of the canopy. We fix the equivalent width of vegetation as $b_e = 1{,}5\,cm$ and subsequently, estimate the canopy frontal area per unit volume (a_v). It was in agreement with the values reported by Abdolahpour et al. (2017a). Additionally, the parameter λ_p was fixed and the drag coefficients were calculated via equation (7.1). Accordingly, the canopy drag length-scale (L_d) is left as an independent parameter, which changes inversely with drag coefficient. Each experiment was forcing by U_∞^{rms} and T according to the table (6.2). The inertia and friction coefficients were fixed, $C_M = 2$ and $C_f = 0{,}05$. The table (7.2) presents the used values.

Table 7.2: Geometric parameters employed during the modelling

	RM	**RH**	**FM**	**FH**
$a_v\,(m)$	9.90	20.5	4.27	9.67
λ_p	0.05	0.103	0.05	0.103
$L_d\,(cm)$	9.6	4.4	22.2	9.3

Canopies with different densities were subjected to identical waves. Significant differences are presented between high-density and medium-density results as shown in figure 7.3. As density increases, the in-canopy velocity attenuation is greater. Notice, for medium density the velocity differences do not exceed $\Delta U = 10\,cm\,s^{-1}$ for experimental data, whereas for high density differences can reach $\Delta U = 16\,cm\,s^{-1}$. Applying a linear fit to the data through the least squares method shows the rigid-vegetation model overestimates dissipation for the high-density cases, $\Delta U < 6{,}1\,cm\,s^{-1}$, otherwise, there is maximum underestimation of the velocity attenuation until $\Delta U = 4\,cm\,s^{-1}$. As a measure of the data dispersion with respect to their trend, the root mean square error ($rmse$) was estimated for both data sets. Similar values were reached for the fit slope (m) and the $rmse$, for the high-density and medium-density

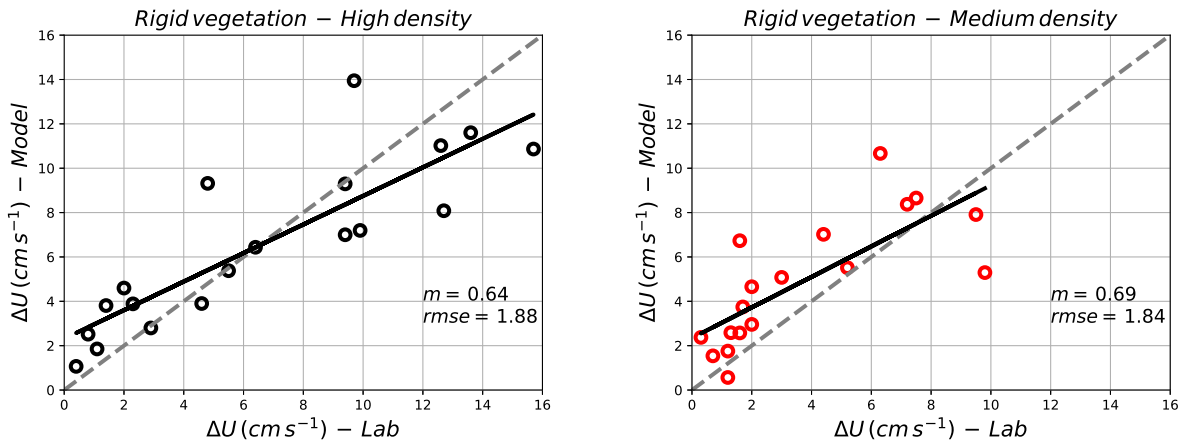

Figure 7.3: Velocity reductions for the rigid vegetation

experiments, $m = 0{,}64$ and $m = 0{,}69$, and $rmse = 1{,}88\,cm\,s^{-1}$ and $rmse = 1{,}84\,cm\,s^{-1}$, respectively. Considering the fits are approximately equal, it is reasonable to consider that the density changes could generate significant variations in calculating in-canopy velocity attenuation. However, this feature is commonly neglected to estimate drag coefficients and their mechanisms of canopy drag modification are still been studied (Etminan et al., 2019). The results also suggest that a better approximation of the C_D can help to improve the model performance.

7.3. In-canopy velocity attenuation by flexible vegetation

Considering the same coefficients as those for the rigid vegetation model ($C_D = eq.\ 7.1$), $C_M = 2$ and $C_f = 0{,}05$), we run the 19 wave experiments considering the flexible vegetation and the developed model. The parameters a_v was obtained considering a equivalent width $b_e = 15\,mm$ and the same vegetation fraction (λ_p) as in the rigid experiments.In the same way, we plot the scatters between measured and modelled velocity differences (ΔU) to identify the performance of the new model. Remarkably, a great improvement was achieve for the high-density experiments. The fitting slope (see fig. 7.4) of the fit is closer to the unit indicating a better agreement with the experimental data. The dispersion has also an improvement reducing to $rmse = 0{,}57\,cm\,s^{-1}$. In the medium-density experiments all the values were under-reduced and a the slope of the fit was $m = 0{,}49$ denoting a poor agreement. However, the adjustment of data to the fit was better than rigid-vegetation conditions, $rmse = 0{,}23\,cm\,s^{-1}$.

Both cases, high-density and medium-density results suggest that a reduction of the C_D is required in order to improve the agreement. The developed model was run for drag coefficients from $C_D = 0{,}01$ to $C_D = 5$ in step of 0,01. After running the developed model the drag

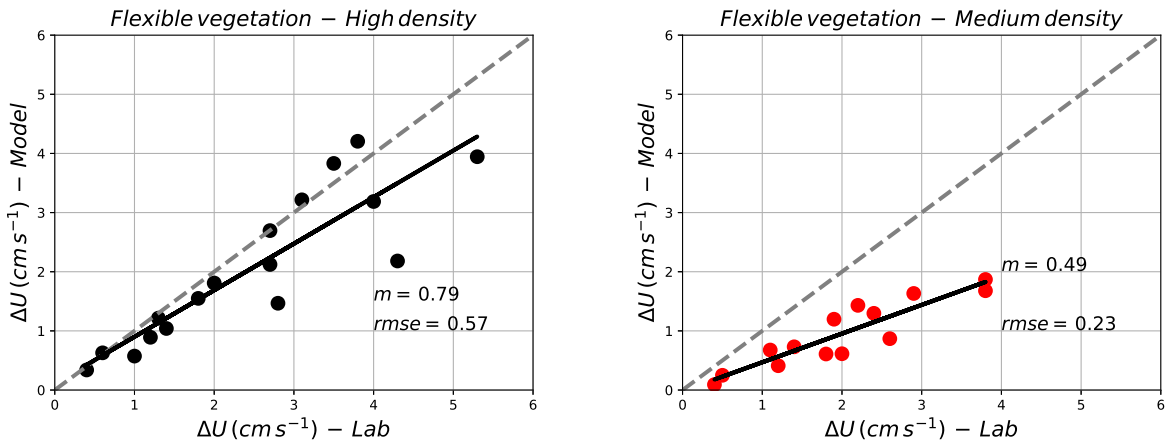

Figure 7.4: Velocity reductions for the flexible vegetation

coefficient associated to the minimum difference of $|\Delta U_{lab} - \Delta U_{model}|$ was selected as the best-fit drag coefficient. The obtained coefficients are presented in the table (7.3).

Table 7.3: Drag coefficients obtained by the fitting procedure for the 19 wave conditions. FH and FM indicate the high and medium density of the flexible cases.

Test	**1**	**2**	**3**	**4**	**5**	**6**	**7**	**8**	**9**	**10**	**11**	**12**	**13**	**14**	**15**	**16**	**17**	**18**	**19**
$C_D - FH$	1.02	1.04	1.52	3.96	1.14	1.01	-	1.18	1.86	1.52	3.30	1.66	1.86	-	1.56	2.00	1.73	1.38	1.61
$C_D - FM$	2.67	3.76	-	3.16	2.31	3.04	-	3.28	4.49	4.73	4.13	2.31	2.19	-	4.73	-	-	3.28	2.19

The drag coefficients present a significant difference between high-density and medium-density experiments. For the first one, drag coefficients range over one, whereas for the second one drag coefficients reach almost five. This difference could be associated to the density, which is the only parameter that changes.

The developed model was run again employing the drag coefficients obtained with the best fit and the results are shown in figure (7.5). As a validation of the drag coefficients, they were compared with equation (7.1). The results for high-density experiments show a properly agreement. However, experiments for the medium density show other kind of pattern. In the literature there are studies that have reported this magnitudes (see Chen et al. (2018)), but it was not possible to obtain attenuation coefficients from them.

7.4. Drag coefficient calculation

Commonly, literature presents multiple equations to characterise the drag coefficient. These approaches are independently implemented and in many cases, there is not a possibility to

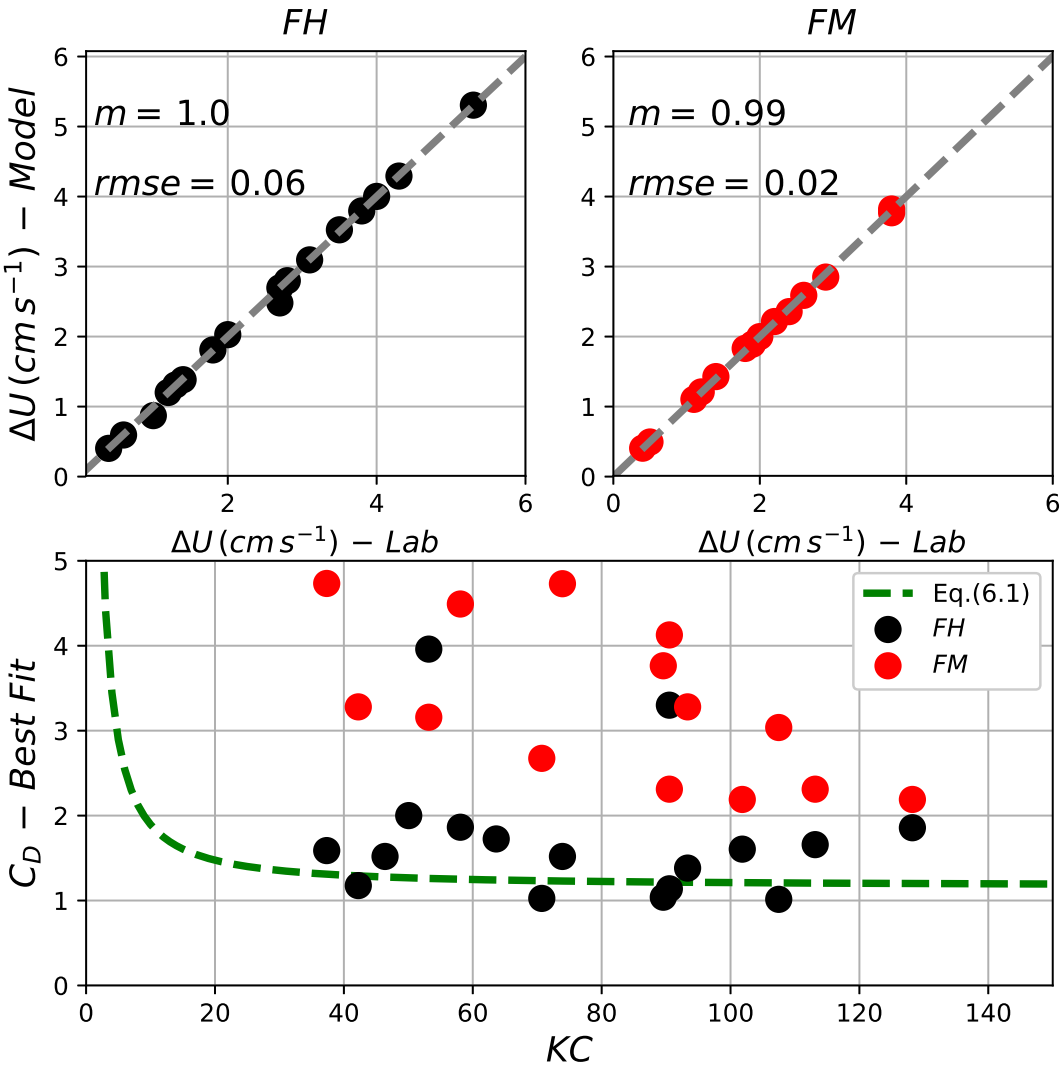

Figure 7.5: Estimated drag coefficients for flexible vegetation

integrate the results and go beyond the particular experiments. The equations are based on the Keulegan–Carpenter number, which relates hydrodynamic features with the element width, assuming that vortex shedding occurs independently because of the interaction of each element. However, for a group of elements, e.g. seagrasses, different mechanism can take place affecting the canopy drag coefficients. For instance, the blockage effect that can be defined as the enhancement of drag forces due to flow past throughout a lateral confined space, for example between seagrass elements. This process is found to be responsible for increasing drag coefficients at high KC for medium to high density canopies as in this study.

Additionally, the sheltering is presented, elements that are located in the wake region of upstream elements experiences a lower incident velocity resulting in a lower drag force and coefficient (Etminan et al., 2019).

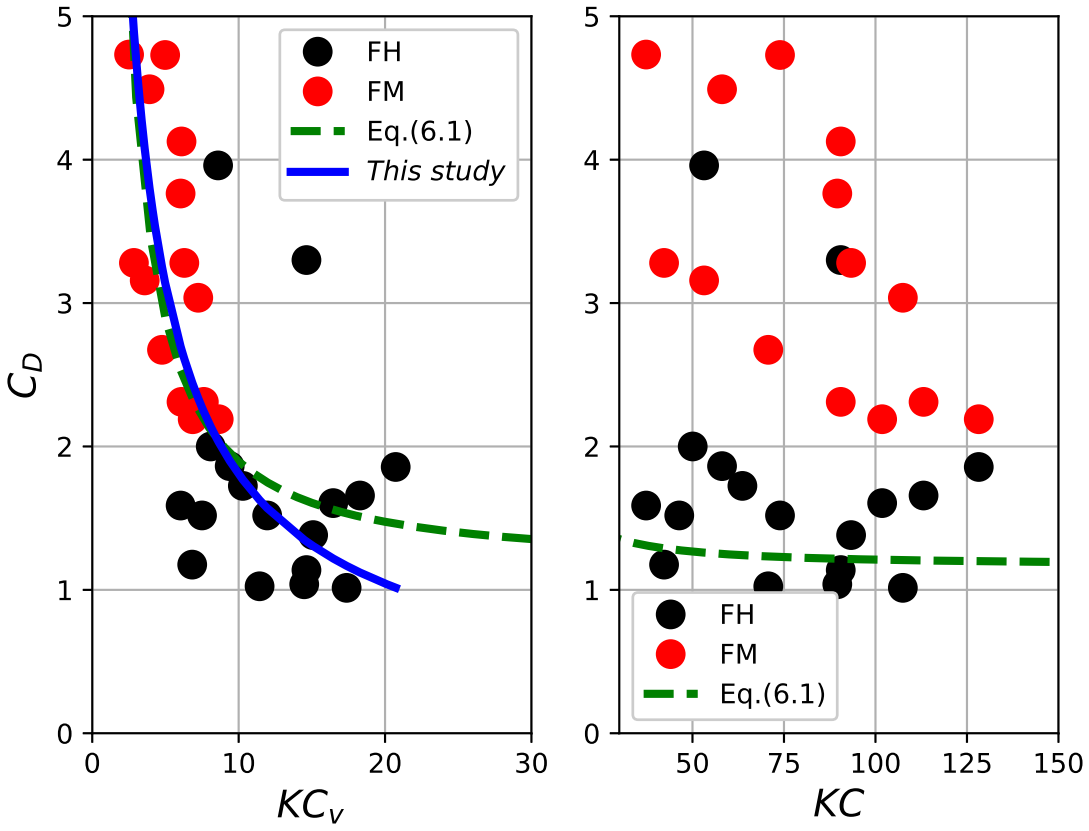

Figure 7.6: Comparison between drag coefficient fits as function of KC and KC_v for flexible vegetation

Considering the density differences between set of experiments it is assuming that the length scale employed to compute KC is defined in terms of a constant drag length scale ($\bar{L}_D$), without taking into account the C_D (Abdolahpour et al., 2017b):

$$KC_v = \frac{U_\infty^{max} T}{\bar{L}_D} \tag{7.2}$$

$$\bar{L}_D = \frac{1 - \lambda_p}{a_v} \tag{7.3}$$

this drag length scale can be seen as a measure of vegetation density defined as the vegetation frontal area per water unit volume. This definition of the Keulegan–Carpenter number is very similar to the one made by Abdolahpour et al. (2018) who assumed a constant $C_D = 1$. For this particular study, the medium-density experiments presents a $\bar{L}_D$ approximately twice as those for high-density conditions. Consequently, the KC_v will be half of the high-density conditions and based on existing formulations for C_D, it is expected to obtain greater drag coefficients.

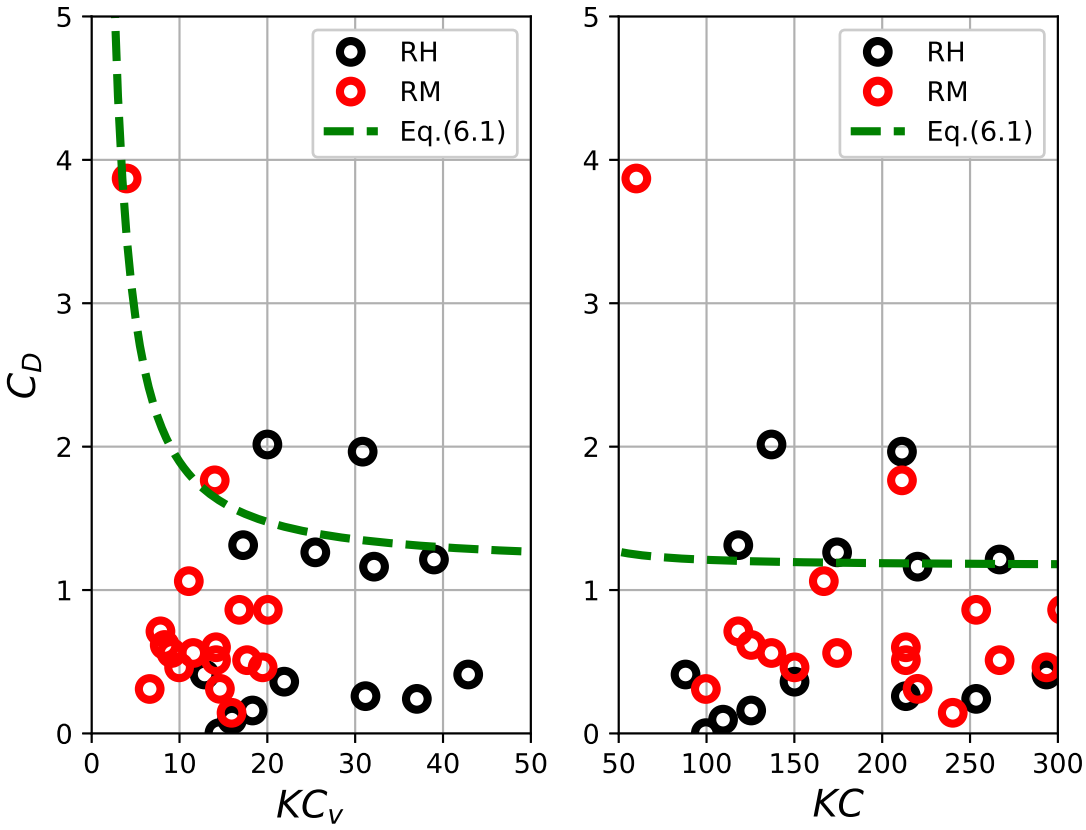

Figure 7.7: Comparison between drag coefficient fits as function of KC and KC_v for rigid vegetation

Employing the definition of the KC_v, we plot it versus the C_D. The results are shown in the left side of the figure (7.6), the right side corresponds to figure (7.5) plotted again to facilitate the comparison. The equation (7.1) is used to identify if data follow a specific pattern. Information for medium density now is fitted to this equation for a different part of the curve in comparison with high-density data. A new fit of the complete data is carried out and is presented here:

$$C_D = 11{,}2KC_v^{-0{,}792}, \quad R^2 = 0{,}59 \qquad 2{,}5 < KC_v < 14{,}6 \tag{7.4}$$

The new fit agrees with the equation (7.1) for $KC_v < 9$. However, $KC_v > 9$ the curve gives smaller values. Following this procedure, we estimate the drag coefficients for the rigid vegetation. In general, they were smaller than those obtained for flexible vegetation, which agrees patterns reported in the literature (Méndez y Losada, 1999; Maza et al., 2013).

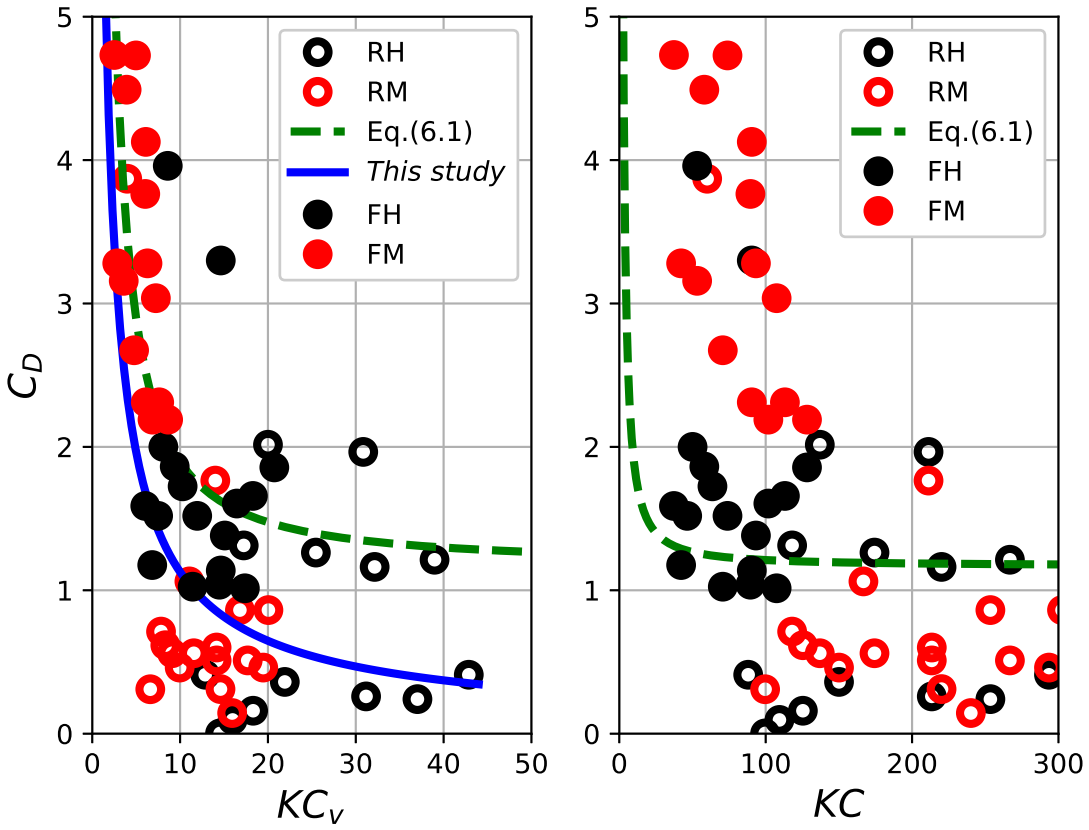

Figure 7.8: Comparison between drag coefficient fits as function of KC and KC_v for all the experiments

In this case, the role of vegetation density was not so clear as in flexible vegetation. For medium and high density, most of drag coefficients exhibit similar values bounded between $0{,}1 - 2$, as right side of figure (7.7) shows. Remarkably, the presentation of drag coefficients in terms of KC_v allow to consider values that apparently seem as out-layers. In the particular case of the coefficient $C_D = 3{,}8$ associated to $KC = 52$ in the right panel exhibits a pattern

extremely different to values with similar KC and reported patterns as equation (7.1). However, in the left panel it is in agreement with the equation(7.1) and can be calculated if any fit is developed for the information. For the rigid conditions we do not estimate a fit for the drag coefficients because they were compiled with data from flexible vegetation to obtain a better representation.

The figure (7.8) shows the drag coefficients for the rigid and flexible vegetation compared with the KC_v. For $C_D > 2$ there is a clear pattern that follows equation (6.1), however, for $C_D < 2$ the variability is higher. We fitted all the drag coefficients and obatained a new empirical expression for both rigid and flexible vegetation:

$$C_D = 10{,}76{KC_v}^{-1} + 0{,}45, \quad R^2 = 0{,}41 \qquad 1 < KC_v < 45 \tag{7.5}$$

The results were compared with the equation (6.1) employing the coefficient of determination (R^2) showing a adjust of $R^2 = 0{,}30$. Information with other spatial densities may be considered extremely useful helping to make the graph longer, validating widely this approach.

7.5. Representation of the in-canopy flow and plant motion

Considering the drag coefficients obtained by the fitting procedure, we analysed the representation of the in-canopy velocity, and the displacement of the plant top and its velocity. All the experiments exhibit the same pattern, a reduction of the amplitude of the in-canopy velocity in comparison with the incident velocity, a slightly delayed lag between the in-canopy velocity and the incident velocity, a in-phase plant velocity with the in-canopy velocity, a local peak in the plant velocity that is overlapping with the zero crossing of the in-canopy velocity and a out of phase plant movement (fig. 7.9).

The computed phase differences between the fluid velocity and plant velocity at the top end of seagrass stem differ with previous reports of Zhu y Chen (2015). That study suggests the phase angle is strongly dependant of the plant stiffness and flow conditions. In tha case, the phase angle goes rapidly from 0° to 90°. However, our results showed that the phase angle is not sensible to the relation between plant stiffness and wave conditions. Another difference is the presence of two marked peaks during the wave cycle in the plant velocity records, which become stronger as long as plant rigidity increases. The displacements of the vegetation top are completely out of phase with the in-canopy velocity.

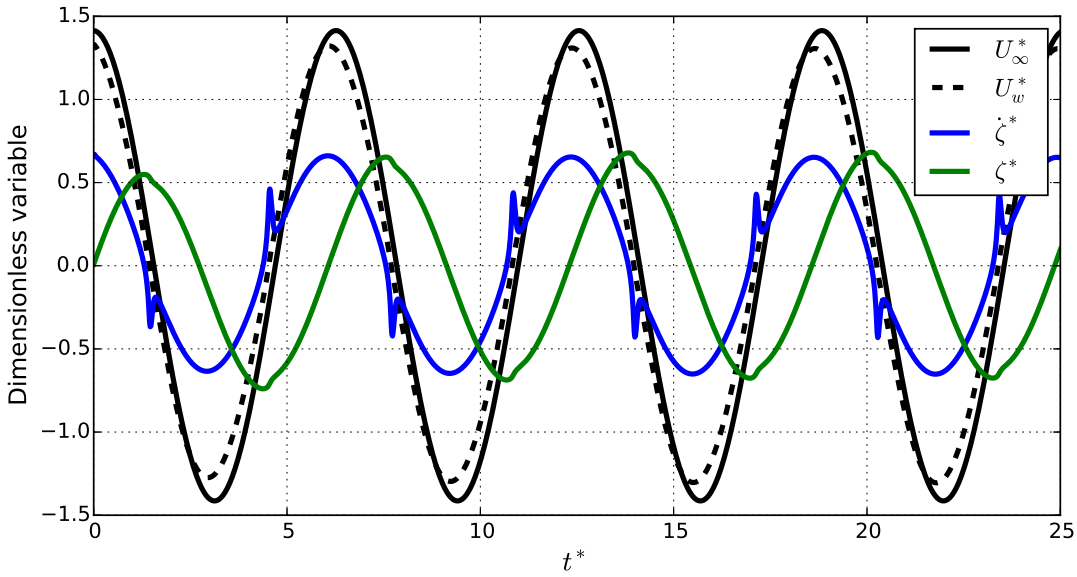

Figure 7.9: Incident (U_∞^*), in-canopy (U_w^*), plant ($\dot{\zeta}^*$) velocities and plant displacement (ζ^*)

8 Discussion and Conclusions

Including plant movement into the numerical formulations generates significant and positive changes in results in comparison with analysis developed with models that assume seagrasses as rigid vegetation. The statistical variability of drag coefficients is reduced and more clear trends in their values are observed.

The capacity of seagrasses to change flow patterns inside the canopy is clearly evidenced through experimental data and modelling results. The vast majority of the state-of-the-art models for studying wave energy dissipation consider the vegetation elements as rigid structures (Dalrymple et al., 1984; Luhar et al., 2010). However, contribution of vegetation flexibility is a key factor in the in-canopy velocity attenuation process. The most recent approaches employ parametrisations to study the effect of vegetation flexibility (Lei y Nepf, 2019; Luhar y Nepf, 2016), instead of modelling the plant movement because of the flow forcing. For the experiments used in this study the coupling between flow and plant governing equations can be classified as successful. The disturbing and restoring forces of plant movement were identified and included in the developed model (Asano et al., 1992; Méndez y Losada, 1999; Maza et al., 2013).

The developed model is in agreement with the most well-known and validated formulation e.g. Morison's equations (Morison et al., 1950; Laya et al., 1984). The procedure to obtain the model was based on the a priori developments of Lowe et al. (2005) y Lowe et al. (2007). Furthermore, new analysis were carried out, which constitute a base line for future studies regarding in-canopy velocity attenuation. The effectiveness of the developed model can be verified by compering with different source of information, which include both rigid and flexible structures (Lowe et al., 2005; Abdolahpour et al., 2018).

The obtained drag coefficients have similar values to the reported ones in the literature (Chen et al., 2018; Mendez y Losada, 2004) and can be implemented in future studies, considering KC_v-based equations. The developed concept of KC_v opens the discussion to explore the implication to classify flow process with this parameter. The effect of vegetation density on in-canopy velocity attenuation is poorly studied in seagrasses so far (Etminan et al., 2019). Although, this study focused on the total amount of velocity reduced within the canopy, the detailed processes to generate it were not addressed here. A complementary description of the velocity profiles would help to improve the understanding of in-canopy velocity attenuation.

As a general conclusion, we can establish that the effect of flexibility of seagrasses on in-canopy velocity attenuation was studied successfully. A detailed description was done for the parameters involved in wave energy dissipation by the interaction with submerged flexible vegetation. In particular, for the objective 1, we identified drag and inertia force as the mechanisms to generate plant motion. Representation of these forces with the modified Morison's equation improved the description of the in-canopy velocity. On the other hand, vegetation employs the inertia, stiffness, damping and buoyancy forces to limit its displacement as much as it can. When the disturbing are greater than restoring forces, plants exhibit a whip-like movement and the developed model do not reproduce correctly the hydrodynamic phenomena. The second objective was accomplished and is supported with the results for the in-canopy velocities and drag coefficients. Several discussions are expected from peers including additional experimental information. Finally, the characteristics assessed in this study include the flexibility, estimated with the parameter $Ca\,L$, and the vegetation density. Physical properties such as blade density or the morphology of seagrass were not include in this study.

Bibliografía

Abdolahpour, Maryam, Magnus Hambleton y Marco Ghisalberti (2017a). "The wave-driven current in coastal canopies". En: *Journal of Geophysical Research: Oceans*.

Abdolahpour, Maryam, Marco Ghisalberti, Paul Lavery y Kathryn McMahon (2017b). "Vertical mixing in coastal canopies". En: *Limnology and Oceanography* 62.1, págs. 26-42.

Abdolahpour, Maryam, Marco Ghisalberti, Kathryn McMahon y Paul S Lavery (2018). "The impact of flexibility on flow, turbulence, and vertical mixing in coastal canopies". En: *Limnology and Oceanography* 63.6, págs. 2777-2792.

Asano, Toshiyuki, Hiroshi Deguchi y Nobuhisa Kobayashi (1992). "Interaction Between Water Waves and Vegetation". En: *Proceedings of 23rd Conference on Coastal Engineering*. Venice, Italy: Coastal Engineering Research Council, págs. 2709-2723.

Bradley, Kevin y Chris Houser (2009). "Relative velocity of seagrass blades: Implications for wave attenuation in low-energy environments". En: *Journal of Geophysical Research: Earth Surface* 114.1, págs. 1-13.

Chakrabarti, S.K. (1987). *Hydrodynamics of Offshore Structures*. Southampton, UK: Press, WIT.

Chen, Hui et al. (2018). "Deriving vegetation drag coefficients in combined wave-current flows by calibration and direct measurement methods". En: *Advances in Water Resources* 122.135, págs. 217-227.

Coceal, O y S E Belcher (2004). "A canopy model of mean winds through urban areas". En: *Quarterly Journal of the Royal Meteorological Society* 130.599, págs. 1349-1372.

Dalrymple, Robert A, James T Kirby y Paul A Hwang (1984). "Wave Diffraction Due to Areas of Energy Dissipation". En: *Journal of Waterway, Port, Coastal and Ocean Engineering* 10.1.

Dean, R. G. y R. a. Dalrymple (1989). *Water Wave Mechanics for Engineers and Scientists*, pág. 353.

Dupont, S., F. Gosselin, C. Py, E. De Langre, P. Hemon e Y. Brunet (2010). "Modelling waving crops using large-eddy simulation: Comparison with experiments and a linear stability analysis". En: *Journal of Fluid Mechanics* 652, págs. 5-44.

Etminan, Vahid, Ryan J. Lowe y Marco Ghisalberti (2019). "Canopy resistance on oscillatory flows". En: *Coastal Engineering*.

Ghisalberti, Marco y Heidi Nepf (2006). "The Structure of the Shear Layer in Flows over Rigid and Flexible Canopies". En: *Environmental Fluid Mechanics* 6.3, págs. 277-301.

Gruber, Renee K, Deborah C Hinkle y W Michael Kemp (2011). "Spatial Patterns in Water Quality Associated with Submersed Plant Beds". En: *Estuaries and Coasts* 34.5, págs. 961-972.

Houser, Chris, Sarah Trimble y Bradley Morales (2014). "Influence of Blade Flexibility on the Drag Coefficient of Aquatic Vegetation". En: *Estuaries and Coasts* 38.2, págs. 569-577.

Ikeda, Syunsuke, Tomohiro Yamada y Yuji Toda (2001). "Numerical study on turbulent flow and honami in and above flexible plant canopy". En: *International Journal of Heat and Fluid Flow* 22.3, págs. 252-258.

Jonsson, I (1966). "Wave boundary layers and friction factors". En: *Coastal Engineering Proceedings*, págs. 127-148.

Keulegan, G.H. y L.H. Carpenter (1958). "Forces on cylinders and plates in an oscillating fluid". En: *Journal of Research of the National Bureau of Standards* 60.5, pág. 423.

Laya, Enrique, Jerome Connor y Shyam Sunder (1984). "Hydrodynamic Forces on Flexible Offshore Structures". En: *Journal of Engineering Mechanics* 110.3, págs. 433-448.

Lei, Jiarui y Heidi Nepf (2019). "Wave damping by flexible vegetation: Connecting individual blade dynamics to the meadow scale". En: *Coastal Engineering* 147.February 2018, págs. 138-148.

Lowe, Ryan J., Jeffrey R. Koseff y Stephen G. Monismith (2005). "Oscillatory flow through submerged canopies: 1. Velocity structure". En: *Journal of Geophysical Research C: Oceans* 110.10, págs. 1-17.

Lowe, Ryan J., James L. Falter, Jeffrey R. Koseff, Stephen G. Monismith y Marlin J. Atkinson (2007). "Spectral wave flow attenuation within submerged canopies: Implications for wave energy dissipation". En: *Journal of Geophysical Research: Oceans*.

Luhar, M y H M Nepf (2016). "Wave-induced dynamics of flexible blades". En: *Journal of Fluids and Structures* 61, págs. 20-41.

Luhar, M., E. Infantes y H. Nepf (2017). "Seagrass blade motion under waves and its impact on wave decay". En: *Journal of Geophysical Research: Oceans*.

Luhar, Mitul y Heidi M Nepf (2011). "Flow-induced reconfiguration of buoyant and flexible aquatic vegetation". En: *Limnology and Oceanography* 56.6, págs. 2003-2017.

Luhar, Mitul, Sylvain Coutu, Eduardo Infantes, Samantha Fox y Heidi Nepf (2010). "Wave-induced velocities inside a model seagrass bed". En: *Journal of Geophysical Research: Oceans*.

Maza, Maria, Javier L. Lara e Inigo J. Losada (2013). "A coupled model of submerged vegetation under oscillatory flow using Navier-Stokes equations". En: *Coastal Engineering*.

Méndez, F e I Losada (1999). "Hydrodynamics induced by wind waves in vegetation field". En: *Journal of Geophysical Research* 104.C8, págs. 18383-18396.

Mendez, Fernando J. e Inigo J. Losada (2004). "An empirical model to estimate the propagation of random breaking and nonbreaking waves over vegetation fields". En: *Coastal Engineering* 51.2, págs. 103-118.

Mirfenderesk, Hamid y Ian R Young (2003). "Direct measurements of the bottom friction factor beneath surface gravity waves". En: *Applied Ocean Research* 25, págs. 269-287.

Moberg, Fredrik Frededrik y Carl Folke (1999). "Ecological goods and services of coral reef ecosystems". En: *Ecological Economics* 29.2, págs. 215-233.

Morison, J R, J W Johnson y S A Schaaf (1950). "The Force Exerted by Surface Waves on Piles". En: *Journal of Petroleum Technology* 2.05, págs. 149-154.

Nielsen, Peter (1992). *Coastal Bottom Boundary Layers and Sediment Transport*. Vol. Volume 4. WORLD SCIENTIFIC, pág. 340.

Pedocchi, Francisco y Marcelo H. Garcia (2009). "Friction coefficient for oscillatory flow: the rough–smooth turbulent transition". En: *Journal of Hydraulic Research* 47.4, págs. 438-444.

Pujol, Dolors, Teresa Serra, Jordi Colomer y Xavier Casamitjana (2013). "Flow structure in canopy models dominated by progressive waves". En: *Journal of Hydrology* 486, págs. 281-292.

Trowbridge, John y Ole Secher Madsen (1984). "Turbulent wave boundary layers: 1. Model formulation and first-order solution". En: *Journal of Geophysical Research: Oceans* 89.C5, págs. 7989-7997.

Yuan, Zhida y Zhenhua Huang (2015). "Morison coefficients for a circular cylinder oscillating with dual frequency in still water: an analysis using independent-flow form of Morison's equation". En: *Journal of Ocean Engineering and Marine Energy* 1.4, págs. 435-444.

Zhu, Ling y Qin Chen (2015). "Numerical Modeling of Surface Waves over Submerged Flexible Vegetation". En: *Journal of Engineering Mechanics* 141.8, A4015001.